ASSOCIATIE EURATOM-FOM

FOM-INSTITUUT VOOR PLASMAFYSICA

RIJNHUIZEN — NIEUWEGEIN — NEDERLAND

November 1987

TRANSPORT CODE STUDIES OF ELECTRON CYCLOTRON HEATING EXPERIMENTS ON TFR

by

E. Westerhof and W.J. Goedheer

Rijnhuizen Report 87-175

This work was performed as part of the research programme of the association agreement of Euratom and the 'Stichting voor Fundamenteel Onderzoek der Materie' (FOM) with financial support from the 'Nederlandse Organisatie voor Zuiver-Wetenschappelijk Onderzoek' (ZWO) and Euratom.

CONTENTS

ABSTRACT.

Transport code simulations are presented for the Electron Cyclotron Heating (ECH) experiments performed on TFR. The simulations cover both the bulk heating and the MHD mode control experiments. For each of three experimentally identified plasma regimes a scaling of the anomalous electron heat conductivity is identified that yields satisfactory fits for the global plasma characteristics and profiles. For the so-called High-Current and Iron-Dominated regimes the corresponding scalings (with $\chi_e \sim T_e^{1/2}$) also yields a satisfactory description with ECH. This was not the case for the Low-Current regime which showed an exceptionally high ohmic confinement and a strong degradation of confinement with ECH. Instead, good simulations of the ECH phases of Low-Current discharges were obtained with the scaling for the High-Current regime. Shifting the electron cyclotron resonance off-axis led to a gradual decrease of confinement in the simulations. This is in contrast with the experimental findings which showed a strong reduction of confinement already when the resonance was displaced by more than + or −5 cm. This discrepancy can be explained by increased radial transport caused by the destabilization of the m=2, n=1 tearing mode as a consequence of the broader profiles that are generated by off-axis heating. Furthermore, simulations of the mode control experiments were performed using the quasi-linear theory for tearing modes. Starting from an ohmic target plasma which was unstable to the m=2, n=1 tearing mode, the evolution of the m=2, n=1 magnetic island during a 100 ms ECH pulse was calculated for various positions of the electron cyclotron resonance and levels of injected power. The best results, i.e. a complete suppression of the island, are obtained for heating almost exactly on the q=2 surface. In contrast to experimental results, the suppression of the island is found to be only temporary. It is concluded that the suppression of the MHD activity obtained in the experiment cannot be explained by profile tailoring alone.

1 INTRODUCTION.

During the last one and a half year of operation of the Tokamak de Fontenay-aux-Roses (TFR) studies on plasma heating by electron cyclotron waves were performed [1-6]. For this purpose TFR was equipped with three 60 GHz gyrotrons, each capable of delivering 200 to 240 kW for 100 ms. The power from the gyrotrons was transferred to the tokamak by transmission lines, which also served to convert the TE_{02}-mode generated by the gyrotrons into the TE_{11}-mode which is almost linearly polarized. This optimizes the coupling to the O(rdinary)-mode which, for propagation perpendicular to the magnetic field, is lineraly polarized, the electric field being parallel to the magnetic field and perpendicular to the wave vector. The overall efficiency of the transmission lines was 70 to 80%. The schematic layout of the transmission lines is given in Fig. 1.

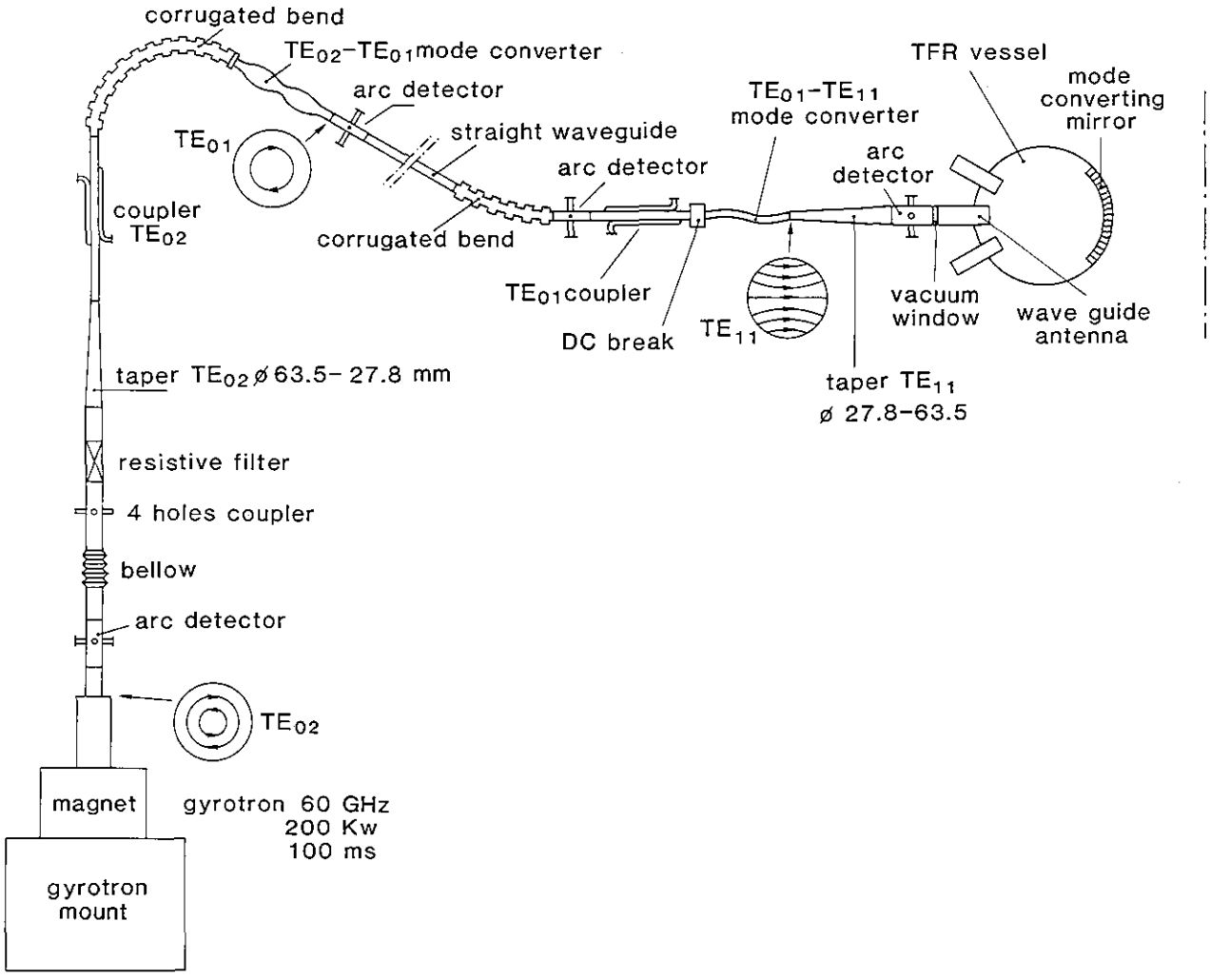

FIG. 1 Schematic layout of a transmission line showing bends, mode converters, and other components. Mode couplers were placed at various positions in the transmission lines to monitor the power flux in the desired mode. Arc detectors were placed at critical points in the lines (e.g. behind bends and mode converters) to detect possible breakdowns in the lines.

The launchers were all directed toward the magnetic axis of TFR, two of them exactly perpendicular and the third with an angle of 74° with respect to the toroidal magnetic field. To prevent power reflection back into the transmission lines in cases of weak wave absorption, a mirror was mounted on the vacuum vessel of TFR opposite to the launchers. During the first experiments this was a smooth, symmetric roof-top mirror, which did not affect the polarization of the wave. Later, this mirror was replaced by a one-sided, grooved mirror which was tilted by 10° and which rotated the polarization over 90°, thus changing the wave from O- to X-mode polarization. Most experiments were performed in the presence of this mode-converting mirror. The launching geometries are sketched in Fig. 2.

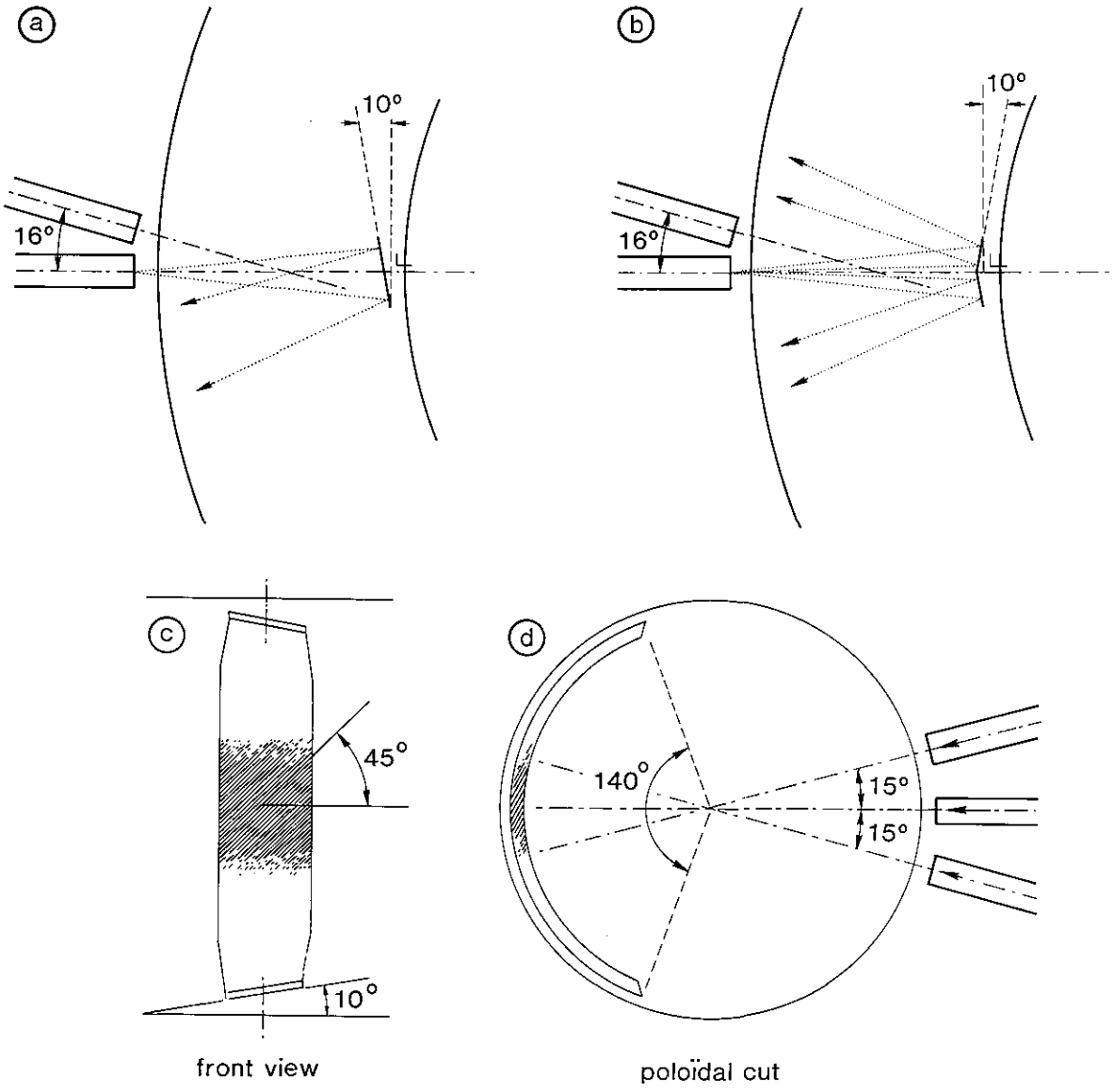

FIG. 2 Sketch of the positions of the antennae and the reflecting mirrors: a), c), and d) refer to the case with the grooved, mode converting mirror, b) refers to the case with the smooth, mode conserving mirror.

A large portion of the available machine time during these last operational periods of TFR was devoted to the Electron Cyclotron Heating (ECH) experiments. Topics addressed in the experiments included, among others, bulk heating and MHD mode control. In this paper, transport code simulations of the experimental results on these two topics are presented.

The main question addressed in the simulations of the bulk heating experiments was the behaviour of the energy confinement with ECH. Scalings are presented for the anomalous electron heat conductivity which yielded satisfactory simulations of the global plasma characteristics in the various plasma regimes both with and without ECH. Little was known so far about the influence of strong additional heating with ECH on the energy confinement, as high power sources in the electron cyclotron range of frequencies became available only recently. Moreover, the first results of high power ECH experiments have yielded contradictory results [7]. From experiments conducted in D-III [8] it was concluded that discharges with ECH show a similar scaling of the energy confinement time as do discharges with Neutral Beam Injection (NBI). In T-10 [9], in contrast, the confinement with ECH was found to be well above that of L-mode scaling [10] which in most other tokamaks applies in the case of NBI. Instead, the confinement in T-10 agrees well with T-11 scaling [11].

The MHD mode control experiments in TFR aimed at the suppression of magnetic islands attributed to instability of the m=2, n=1 resistive tearing mode. This suppression is thought to be due to local changes in the temperature and, consequently, in the current density profiles induced by suitably localized ECH. In the simulations this interpretation of the experiments was investigated using the quasi-linear theory of tearing modes [12].

The organization of the paper is as follows. In the next section a short description of the transport code used, ICARUS, is given. Also the ECH model used in the simulations of the bulk heating experiments, is described and compared with full ray-tracing calculations. The subsequent two sections deal with ECH bulk heating and MHD mode control. These sections are self-contained: first, the relevant experimental data are shortly reviewed, and thereafter the results of the simulations are presented and discussed. In a final section the results are summarized.

2 INTRODUCTION TO THE TRANSPORT CODE.

In this section a description of the version of the 1-D(imensional) transport code ICARUS [13] used for the present work, is given. In the first part the ICARUS code is presented and the underlying physical models and assumptions are described shortly. In the second part a simple model, saving large amounts of computing time, for the calculation of the deposition of the ECH power is described and compared with results from full ray-tracing calculations.

2.1 ICARUS.

The magnetic field lines of a tokamak form a set of nested surfaces, which are well represented by a set of concentric circles. Because the transport along the magnetic field is very much faster than the transport across the magnetic field, the longest transport timescale is that for radial transport. On this timescale the basic plasma variables, e.g. electron and ion densities and temperatures, are constant over a magnetic surface and are, thus, only a function of the radius. The evolution of the corresponding radial profiles is given by a system of coupled diffusion equations

$$\frac{\partial}{\partial t} u_i = \sum_j \frac{\partial}{r\partial r} r D_{ij} \frac{\partial}{\partial r} u_j + S_i , \tag{1}$$

where the u_i are the plasma variables, the D_{ij} are the corresponding transport coefficients, and the S_i are the sources (or sinks). The ICARUS code solves Eq. (1) for the vector $\mathbf{u}$ comprising the poloidal magnetic field B_θ, the electron density n_e, the density of specific light and heavy impurities n_I and n_Z, respectively, and the electron and ion pressures p_e and p_i. The ion pressure contains the contributions from all ion species, which at each radius are assumed to have equal temperatures, i.e. $p_i = (\Sigma_l n_l) \cdot kT_i$ where l runs over all ion species.

The ICARUS code contains a variety of models describing physical phenomena that play a role in the behaviour of a tokamak discharge. From these models any selection can be made by setting appropriate switches in the code. Keeping only the dominant contributions to the transport equations as used in the present simulations, the equations can be written as follows:

For the poloidal field we used

$$\frac{\partial}{\partial t} B_\theta = \frac{\partial}{\partial r} \frac{\eta}{\mu_o r} \frac{\partial}{\partial r} r B_\theta, \tag{2a}$$

where η is the resistivity and μ_o the permeability of vacuum. The classical Spitzer resistivity was used neglecting corrections due to trapped particles.

For the electron density we used

$$\frac{\partial}{\partial t} n_e = -\frac{\partial}{r\partial r} r\Gamma_n + S_n \qquad (2b)$$

$$\text{with } \Gamma_n = -D_n \partial/\partial r(n_e) - n_e v_{pinch},$$

where D_n is the anomalous diffusivity of the electrons, v_{pinch} is the inward pinch velocity including the inward pinch predicted by collisional transport theory (the so-called 'Ware-pinch' [14]), and a possible anomalous pinch velocity v_a, and S_n is the particle source including electrons coming from ionization of neutral particles and the net effect of changes in the degree of ionization of impurity ions. Under most circumstances this latter contribution will be negligible compared to the source from ionization of neutral particles. The model employed in ICARUS to calculate the source from ionization of neutral particles requires some additional remarks. First it is supposed that a fraction R of the particle flux at the edge is neutralized and reenters the plasma. In all calculations R = 1 will be used, i.e. the particle content of the plasma is supposed to be constant. Because the neutral particle transport is fast compared to the radial plasma transport, one can calculate the neutral particle distribution in quasi-steady state. This means that instantaneously a neutral particle distribution is set-up such that equal amounts of neutrals are being ionized in the plasma as are being formed at the edge. In ICARUS this neutral particle distribution is calculated in a plane slab model, which in principle is valid if the mean free path of the neutrals in the plasma is small compared to the minor radius. It must be noted that for the plasma conditions typical of the ECH experiments in TFR this requirement is only marginally fulfilled. Therefore, conclusions regarding the density behaviour will have to be taken with some care.

For the electron pressure we used

$$3/2 \frac{\partial}{\partial t} p_e = -\frac{\partial}{r\partial r} r (Q_e + 5/2 \Gamma_n kT_e) + P_\Omega + P_{ECH} - P_{ei} - P_{rad} \qquad (2c)$$

$$\text{with } Q_e = -n_e \chi_e \partial/\partial r(kT_e),$$

where χ_e is the anomalous electron heat conductivity, P_Ω is the power source due to ohmic heating, P_{ECH} is the Electron Cyclotron power source to be discussed in the second part of this section, P_{ei} is the collisional energy exchange between the electrons and the ions, and P_{rad} includes all radiation losses. The calculation of the radiation losses includes bremsstrahlung, cyclotron radiation and line radiation of the impurity ions. For plasma parameters typical of the ECH experiments in TFR the dominant contribution comes from impurity line radiation which can only be calculated in an approximate manner. A satisfactory approximation is provided by the corona model in which all transport effects of ions in various ionization states are neglected, excitation is by collisions with electrons and de-excitation is radiative.

For the ion pressure we used

$$ {}^{3}/_{2} \frac{\partial}{\partial t} p_i = - \frac{\partial}{r \partial r} r Q_i + P_{ei} \qquad \text{with } Q_i = -n_i \chi_i {}^{\partial}/_{\partial r}(kT_i), \tag{2d} $$

where χ_i is the ion heat conductivity taken from collisional theory [14], i.e. no anomalous ion heat conductivity has been used.
The light and heavy impurities, finally, are specified at the beginning of each simulation and are assumed not to change with time.

The anomalous transport coefficients χ_e, D_n, and v_a are a key topic in tokamak plasma physics and the main subject of Section 3. Ref. [15] gives a comprehensive review of anomalous transport in tokamaks. Here we limit ourselves to some general remarks.
Generally the anomalous heat conductivity is represented by a scaling of the type

$$ \chi_e = \left(\Pi_j v_j^{\alpha_j} \right) F(r) \tag{3} $$

where the v_j are plasma variables, e.g., the major radius R, the minor radius a, the electron temperature T_e, the electron density n_e, the safety factor q, etc., and F(r) is some function of the radius. In the section on bulk heating scalings for χ_e are presented which fitted the experimental results from the various plasma regimes. Because the particle confinement time is generally several times longer than the energy confinement time but obeys a similar scaling, D_n is usually taken to be proportional to χ_e. We used $D_n = {}^{1}/_{4} \chi_e$. To obtain the correct electron density profile normally an anomalous inward pinch velocity is needed. For this the form

$$ v_a = v_o (r / a)^2 \tag{4} $$

was taken. The anomalous pinch velocity was kept constant during a discharge.

2.2 THE ELECTRON CYCLOTRON HEATING MODEL.

The propagation of electromagnetic waves in the electron cyclotron range of frequencies can be described in terms of the WKB approximation; the wave lengths involved (e.g., $\lambda = 5$ mm at a frequency of 60 GHz) are short compared to typical scale lengths in a tokamak (e.g., the minor radius which in the case of TFR is a = 18 cm). Furthermore, the dispersion properties and the linear absorption of electron cyclotron waves are well known [16]. Ray-tracing techniques therefore can provide accurate calculations of the electron cyclotron power deposition profile, P_{ECH}, required in the transport code simulations. This approach, however, requires long computing times. For this reason we used a simpler model in the transport code calculations for the bulk heating experiments, similar to the model described in Ref. [17]. This model is motivated by the observation that the layer where the power is absorbed, is thin compared to the radius of curvature of the ray trajectories caused by refraction. Consequently, within this layer refraction may be neglected. This allows to approximate the actual rays by a straight beam, the width of which is chosen in such a way that it accounts for the refraction of the rays along their paths up to the absorption layer. The power density in vertical direction, y, of the beam is taken to be parabolic, i.e. for $|y - y_o| \leq w$

$$P_{beam}(y) = P_o (1 - (y - y_o)^2 / w^2), \tag{5}$$

where w is the half-width of the beam and y_o is the vertical position of the centre of the beam at the absorption layer. A projection of the rays on the poloidal plane results in a local power absorption given by

$$P_{abs} = \alpha(x, y)\, P_{beam}(y) \exp - \int_o^{s(x, y)} \alpha(s')\, ds', \tag{6}$$

where x is the coordinate along the major radius, s' is the coordinate along the ray trajectory, and $ds' = dx / \sin\theta$, $\theta = \text{atan}\, |N_\perp / N_\parallel|$, and $N_\perp$ ($N_\parallel$) is the ray-refractive index perpendicular (parrallel) to the magnetic field. In plane slab geometry $N_\parallel$ is constant along a ray. Because this also holds, to a good approximation, in a tokamak, we assumed $N_\parallel$ to be constant along a ray. The power is spread very fast over the whole flux surface affected, yielding a radial power deposition profile

$$P_{ECH}(r) = \frac{1}{4\pi^2 R} \int_o^{2\pi} d\theta\; P_{abs}(x, y). \tag{7}$$

This model gives a satisfactory approximation for P_{ECH} over a wide range of plasma parameters, for injection of the O-mode from the high- and low-field side as well as for the injection of the X-mode from the high-field side, if the angles of propagation are not too far from perpendicular with respect to the toroidal field. Also the power absorbed along rays reflected by a mirror mounted on the discharge chamber opposite to the wave guide antennae can be accounted for. In this case Eq. (6) has to be applied also to the reflected rays with $N_\parallel$ being determined by the reflection of the ray at the mirror. For densities close to or above cut-off, of course, the refraction effects are large

and the model is no longer valid. Figure 3 gives P_{ECH} as calculated with this model for typical plasma parameters. For comparison also the results of a full ray-tracing calculation with the TORAY code [18] are given. Clearly, the results obtained with the simple model agree well with the full ray-tracing calculations.

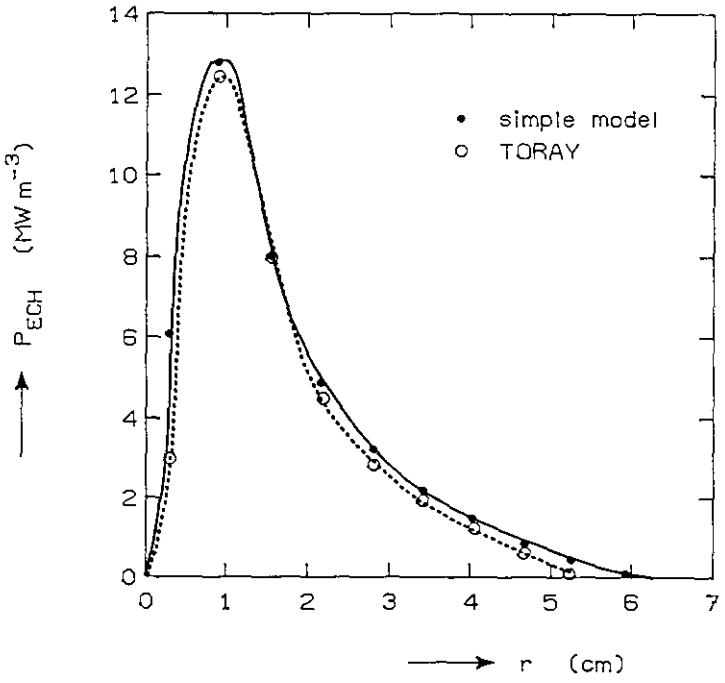

FIG. 3 Power deposition profiles as calculated by the simple model (full lines) and by a full ray-tracing calculation. In both cases 200 kW of 60 GHz waves in the O-mode was injected perpendicularly to the toroidal field ($N_{||} = 0$) into a plasma with central resonance, R=0.96 m, a=0.18 m, $n_e = 2.5\ 10^{19}\ (1 - (r/a)^2)\ m^{-3}$, and $T_e = 1.0\ (1 - (r/a)^2)^2$ keV. In the simple model a half width of the beam of 6 cm was used. In the ray-tracing calculations the rays were chosen to model a Gaussian beam with an angular spread of 3^0 coming from R=1.5 m, which gives a good representation of the actual antenna pattern.

3 BULK HEATING.

3.1 SUMMARY OF THE EXPERIMENTAL RESULTS.

A main aim of the Electron Cyclotron Heating experiments on TFR was bulk plasma heating. Both plasma variables and heating power were varied over a broad range. The ECH was localized at various positions in the plasma.

In the experiments three distinct regimes of the Ohmic target plasma were found, depending on the plasma current or the contamination with heavy impurities [4-6]. Two regimes corresponded to relatively clean plasma conditions: one for low plasma current (the Low-Current regime with for the safety factor at the edge: $q_a \geq 3.2$) and the other for high plasma current (the High-Current regime with $q_a \leq 3.2$) [2,3,6]. A third regime was present in discharges with a high level of metallic impurities (the Iron-Dominated regime) [4,6]. The latter discharges were obtained during a period in which a calorimeter was installed in the limiter shadow. No dependence of the plasma regime on current was found in the Iron-Dominated regime. The best confinement was obtained in the Low-Current regime which was free of any MHD activity. In the High-Current regime the confinement was degraded by a factor of 1.5 to 2.0 [5]. Other marked differences with respect to the Low-Current regime were the presence of strong, saturated MHD oscillations and a stronger peaking of the T_e-profile. These differences are illustrated in Fig. 4 showing the evolution of the current, line-integrated density, and MHD activity. Also the corresponding temperature and density profiles are shown. In the Iron-Dominated regime the worst confinement was found [5].

In the experiments the central electron density $n_e(0)$ was varied from 1.0 to 5.0 10^{19} m^{-3}. We will concentrate here on the medium-density range ($n_e(0)$ = 1.5 to 3.0 10^{19} m^{-3}) because at low densities strong suprathermal effects were observed during ECH, while at high densities the plasma core was inaccessible for the O-mode, the cut-off density for 60 GHz being 4.46 10^{19} m^{-3}. For these medium densities, the energy confinement was proportional to the density. This remained true also during ECH, although this fact was obscured by strong effects of ECH on the particle content and on the density profile. During ECH the density profile was broadened. In addition, at higher densities a strong density pump-out was observed, while at low densities ECH led to an increase of the total particle content. Figure 5 summarizes the experimental data on central ECH by giving the energy confinement time τ_E as a function of input power for typical medium-density discharges (i.e., with a volume average densitiy $\langle n_e \rangle$ between 1.0 and 1.5 10^{19} m^{-3}) from all three regimes.

Shifting the electron cyclotron resonance to the high- or low-field side leads to off-axis heating. Shifting of the resonance by more than 5 to 6 cm led to a strong degradation of confinement [5]. Smaller shifts, on the other hand, led to only a minor degradation of confinement.

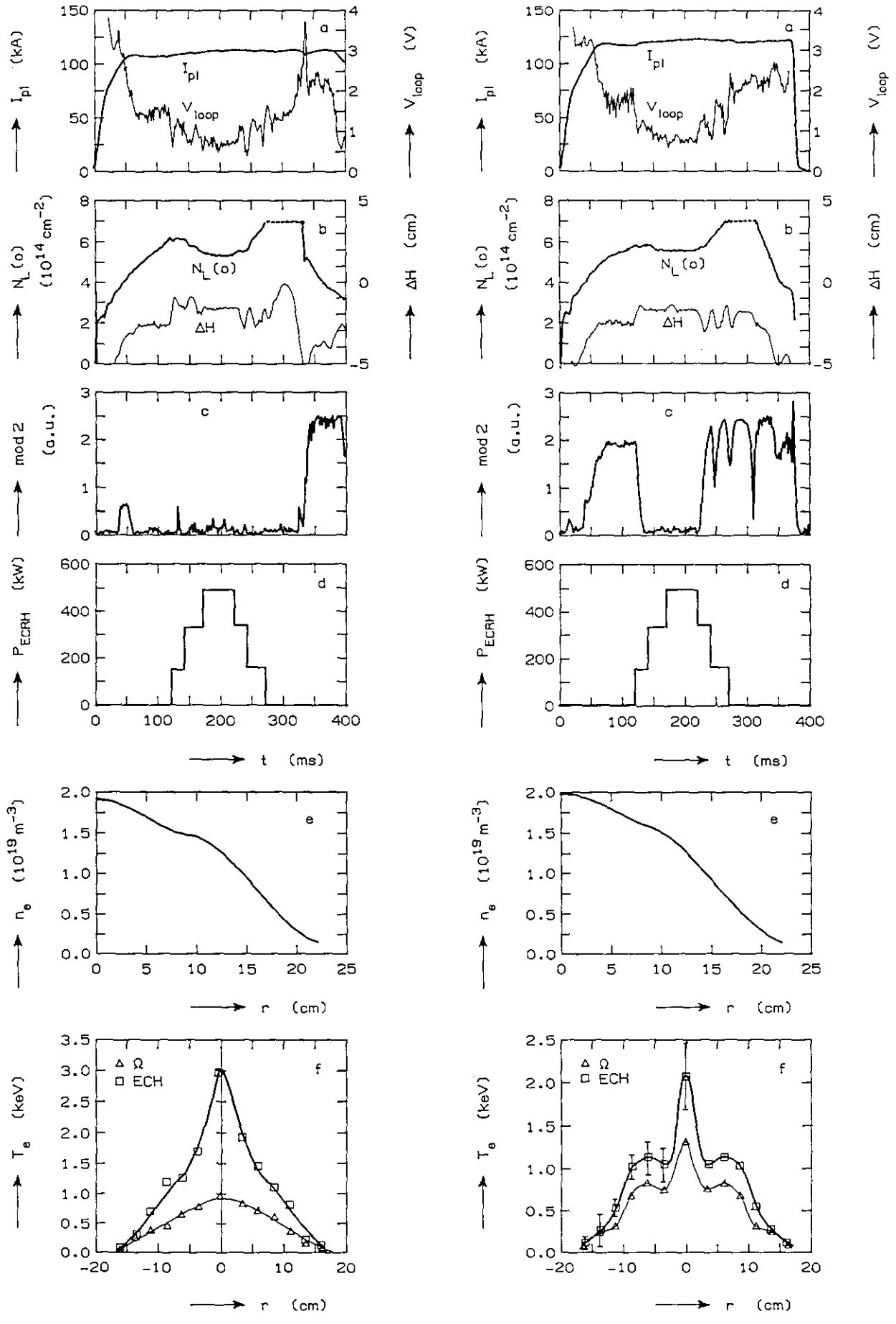
a
I_{pl} (kA)
V_{loop} (V)
b
$N_L(o)$ (10^{14} cm^{-2})
ΔH (cm)
c
mod 2 (a.u.)
d
P_{ECRH} (kW)
t (ms)
e
n_e (10^{19} m^{-3})
r (cm)
f
T_e (keV)
Ω
ECH
r (cm)

FIG. 4 Typical experimental results for a Low- (left) and a High-Current (right) discharge.
a) The evolution of the plasma current I_p and the loop voltage V_{loop}.
b) The evolution of the central line-integrated electron density $N_L(0)$ and the horizontal displacement ΔH of the centre of the plasma column with respect to the centre of the vacuum vessel (R=0.98 m).
c) The evolution of the m=2 mode activity.
d) The injected ECH power.
e) A typical density profile during ECH.
f) Typical temperature profiles both for phases with only ohmic heating and during phases with full power (~500 kW) ECH.

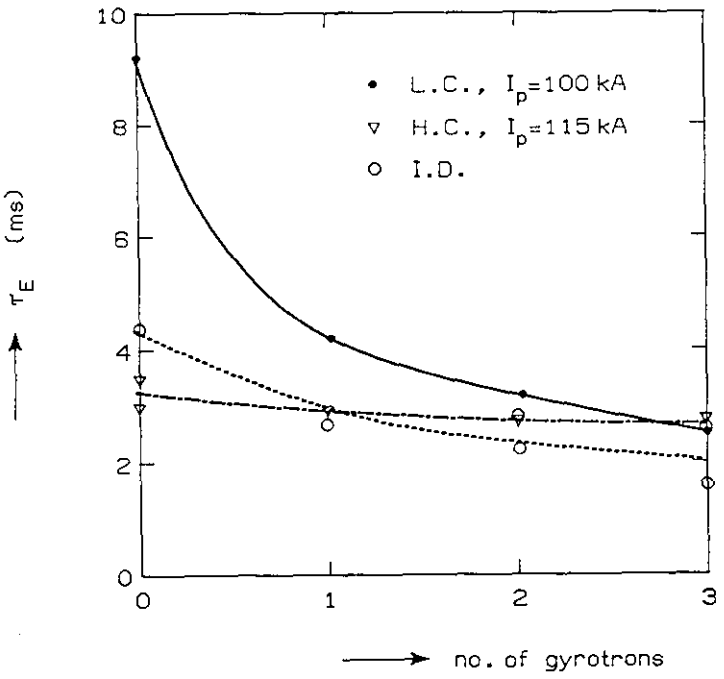

FIG. 5 The energy confinement times as a function of ECH power (each gyrotron corresponds to ~170 kW) for typical medium density (i.e. $\langle n_e \rangle$ = 1.0 to 1.5 10^{19} m^{-3}) discharges from the three regimes [5]. It is noted that the points for the Iron-Dominated regime correspond to dicharges with relatively high densities for which a significant particle pump-out was observed which, at least partly, explains the strong degradation of confinement observed in this case [5].
• Low-Current, $I_p \approx 100$ kA.
▽ High-Current, $I_p \approx 115$ kA.
o Iron-Dominated.

3.2 RESULTS AND DISCUSSION OF THE SIMULATIONS.

The main objective of the simulations was to find a scaling for the anomalous electron heat conductivity which gives a satisfactory description of the energy confinement and of the T_e-profiles observed with and without high power ECH for the discharges investigated. A second question for which we sought an answer in the simulations, was the cause of the differences between the two ohmic regimes under clean plasma conditions.

In search of a proper scaling for the electron heat conductivity χ_e, we observe the following points. First, as is generally observed in tokamaks, the energy confinement in all ohmic regimes was proportional to the density. This justifies the working hypothesis $\chi_e \sim n_e^{-1}$. Secondly, some degradation of confinement was found for high-power ECH. One way to obtain such a degradation is to suppose that χ_e increases whith temperature during ECH. Guided by the results obtained on T-10, we put $\chi_e \sim T_e^{1/2}$. Finally, it is known that the fairly peaked T_e-profiles as observed in tokamaks, generally require a radial profile of χ_e that increases sufficiently strong with radius. To assure such a profile of χ_e, we introduced an explicit radial dependence, viz.

$$\chi_e(r) = \text{Const.} \frac{T_e(r)^{1/2}}{n_e(r)} F(r/a), \tag{8}$$

where, for each regime, the constant was adjusted such that the correct value of the global energy confinement time in the ohmic phase was reproduced, while F(r/a) was chosen such that the experimental T_e-profile was satisfactorily fitted.

For each regime a discharge of medium density was simulated.

The Low- and High-Current Regimes.

For the Low- and High-Current regimes good simulations of the properties of ohmic dicharges were obtained with the following scalings for the electron heat conductivity:

$$\text{at Low-Current} \quad \chi_e = 1.4\ 10^{19} \frac{T_e^{1/2}}{n_e} e^{3((r/a)^4 - 1)}\ m^2/s, \tag{9a}$$

$$\text{at High-Current} \quad \chi_e = 1.4\ 10^{19} \frac{T_e^{1/2}}{n_e} e^{3((r/a)^2 - 1)}\ m^2/s, \tag{9b}$$

where T_e is in eV and n_e is in m^{-3}. The particle diffusion coefficient was $D_n = 1/4\ \chi_e$ while no anomalous inward pinch was required to obtain a good simulation of the density profile. For large r, transport was limited to 5 times Bohm transport: i.e., $\chi_e \leq 5\ \chi_B$ with

$$\chi_B = \frac{T_e}{16\ B}\ m^2/s \tag{10}$$

with T_e in eV and B in Tesla. One discharge at medium density, $\langle n_e \rangle = 1.3\ 10^{19}\ m^{-3}$, in both the Low- and High-Current regime was simulated. In Table 1 the main results of these simulations are given together with experimental results of two corresponding discharges. The T_e and n_e profiles are shown in Fig. 6 including experimental data. Note that the only difference in χ_e for the Low- and High-Current regimes is in the explicit radial function F(r). This is sufficient to explain the difference in both T_e-profiles and energy confinement times. The difference in the functions F(r) and, consequently, in χ_e is largest for $r \approx 0.7$ a. Around this radius the scaling for the High-Current regime results in a value for χ_e which is twice as high as the value given by the scaling for the Low-Current regime. Note, that this radius is close to the q=2 surface, which suggests that the increased transport in the High-Current regime can be attributed to the high level of MHD activity, and more particularly to the m=2, n=1 mode on the q=2 surface, observed only in this regime.

TABLE 1 Plasma parameters and results of the simulations (SIM) for the ohmic High- and Low-Current regimes. Experimental data (EXP) are given for comparison.

		LOW-CURRENT		HIGH-CURRENT	
		EXP	SIM	EXP	SIM
Plasma parameters					
R	(m)	~0.96	0.96	~0.96	0.96
a	(m)	~0.18	0.18	~0.18	0.18
B_z	(T)	2.14	2.14	2.14	2.14
I	(kA)	< 110.	105.	> 110.	115.
$\langle n_e \rangle$	(10^{19} m^{-3})	1.0- 1.5	1.3	1.0- 1.5	1.3
Impurities					
Oxygen		3%	3%	3%	3%
Iron			0.2‰		0.2‰
Ohmic results					
$T_e(0)$	(eV)	~900.	940.	~1000.	980.
$T_i(0)$	(eV)	~300.	315.	~300.	285.
$n_e(0)$	(10^{19} m^{-3})	~2.5	2.6	~2.5	2.6
τ_E	(ms)	~8.	7.0	~4.	4.4
Z_{eff}		~2.0	2.4	~2.0	2.4
V_{loop}	(V)	1.5	1.5	2.0	1.9

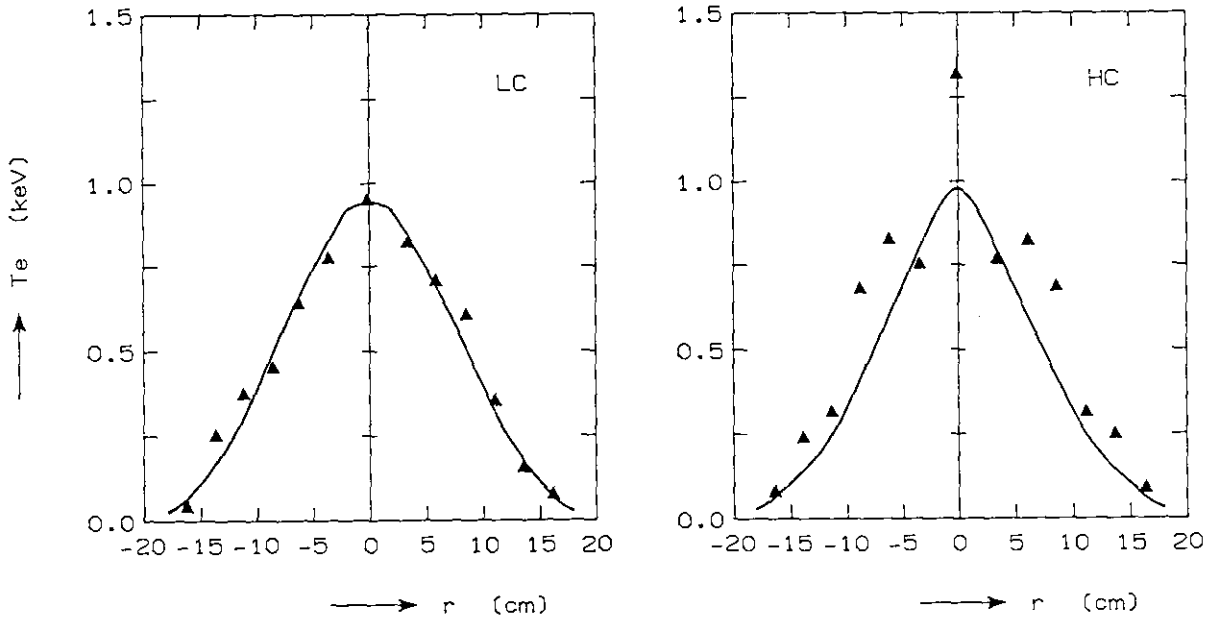

FIG. 6 The ohmic T_e-profiles as obtained in the simulations for the Low- (LC) and the High-Current (HC) regimes (cf. Table 1). Typical experimental data are given for comparison.

We looked for an explanation of the presence or absence of the m=2, n=1 mode in terms of the linear theory of (resistive MHD) tearing modes. The parameter describing instability, Δ', depends only on the current profile and can be calculated easily [19] (see also Section 4.2). This was done for current profiles predicted by the transport code for discharges in both the Low- and High-Current regimes. The current profiles predicted for the High-Current regime were found to be more stable than the current profiles predicted for the Low-Current regime. Also increasing the current in the Low-Current regime led to a decrease of Δ', i.e. an increase of stability. It is difficult, however, to draw definite conclusions from these results, since the absence of experimental data on the current profile leaves large uncertainties. Still we tend to conclude tentatively that the destabilization of the m=2, n=1 tearing mode in the transition from the Low- to the High-Current regime cannot be explained by standard linear theory. A possible alternative explanation is that the m=2, n=1 tearing mode is driven non-linearly unstable by the ideal m=3 surface kink mode, which is expected to be unstable for values of q_a close to 3 (see e.g. [20]).

The scaling for the High-Current regime also yielded good results with central ECH. This is illustrated by Fig.s 7 and 8. Figure 7 presents the temperature profiles as predicted by the High-Current scaling for central ECH with 1, 2, and 3 gyrotrons (~170 kW each) for a discharge with the same parameters as in Table 1. Figure 8 gives the resulting confinement times as a function of total input power. Also given in this picture are corresponding results obtained with the Low-Current scaling. The latter clearly do not reproduce the strong confinement degradation observed experimentally in the Low-Current regime even at quite low ECH power levels. As is seen from Fig. 8, however, these results can be satisfactorily simulated with the High-Current scaling. Thus, we conclude that ECH makes the plasma conditions of the Low-Current regime equal to those of the High-Current regime.

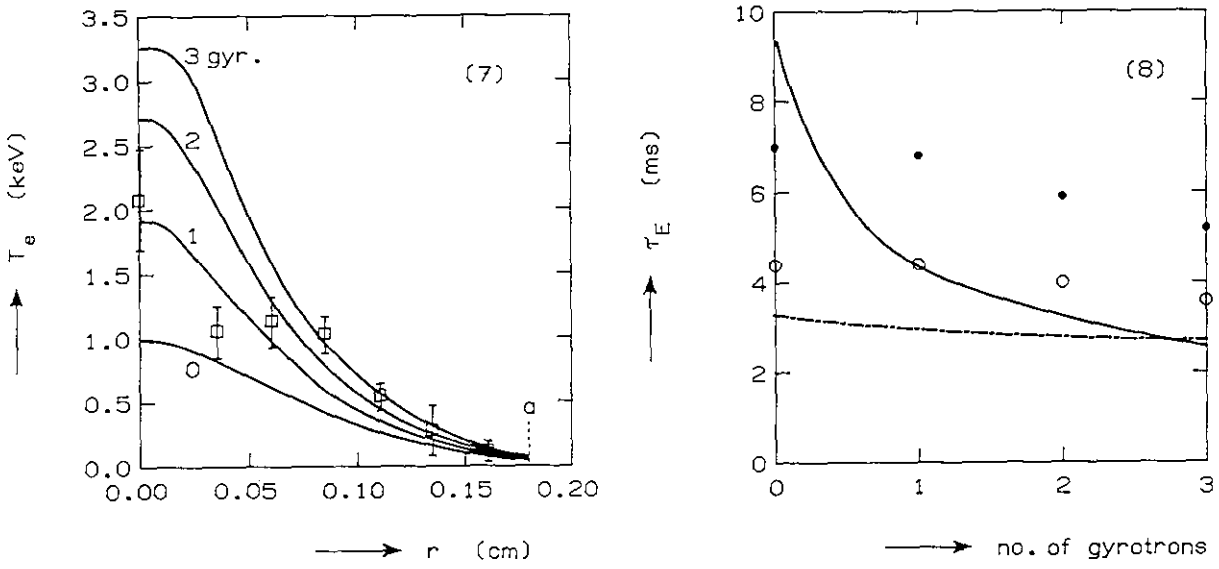

FIG. 7 The T_e-profiles as obtained in the simulations for the High-Current regime during ECH with 1, 2, and 3 gyrotrons (170 kW each). Typical experimental data are given for comparison. Note that simulation and experiment agree well in the outer regions, whereas they differ close to the centre, where the experimental data show a large scatter.

FIG. 8 The energy confinement times during ECH as obtained in the simulations with the Low- (•) and the High-Current (o) scaling for χ_e. The full and the dashed-dotted lines indicate experimental data (cf. Fig. 5) for discharges from the Low- and High-Current regimes, respectively. Note that with ECH the results obtained with the High-Current scaling agree well with the data for both plasma regimes.

The Iron-Dominated Regime.

The Iron-Dominated regime showed a slightly degraded confinement compared with the High-Current regime [5,6]. Good simulations for the Iron-Dominated regime were obtained with the following scaling for the electron heat conductivity

$$\chi_e = 1.2\ 10^{19}\ \frac{T_e^{1/2}}{n_e}\ e^{2((r/a)^2 - 1)}\ m^2/s, \qquad (11)$$

which is very similar to the scaling for the High-Current regime. Only in the central region χ_e is about twice as large. We simulated two discharges in this regime: one at medium density, $\langle n_e \rangle = 1.2\ 10^{19}\ m^{-3}$, and one at high density, $\langle n_e \rangle = 2.1\ 10^{19}\ m^{-3}$. The results for both are presented in Table 2. In Fig. 9 the corresponding T_e-profiles are given for the ohmic phase and for full power (~500 kW) ECH.

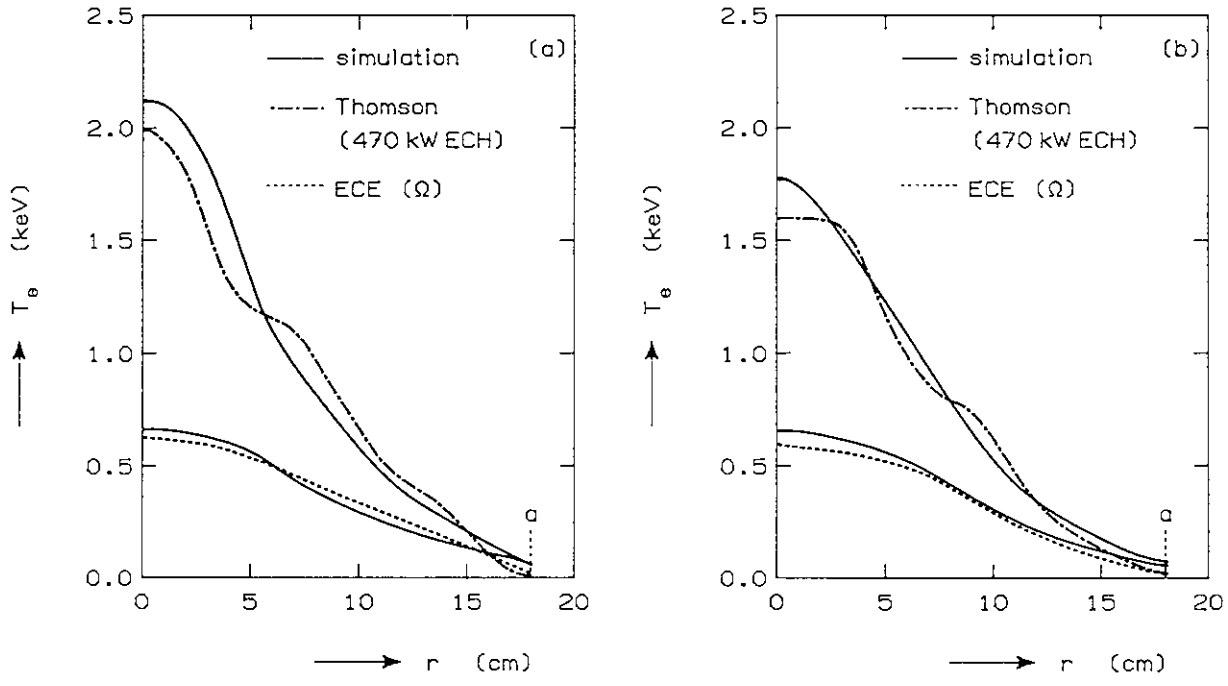

FIG. 9 Results of simulations of discharges from the Iron-Dominated regime. The T_e-profiles both before and during ECH (470 kW) are given for a medium-density (a) and a high-density discharge (b). The other data on these discharges are given in Table 2.

TABLE 2 Plasma parameters and results of the simulations for two discharges from the Iron-Dominated regime.

		MEDIUM-DENSITY		HIGH-DENSITY	
		EXP	SIM	EXP	SIM
Plasma parameters					
R	(m)	0.96	0.96	0.96	0.96
a	(m)	0.18	0.18	0.18	0.18
B_z	(T)	2.14	2.14	2.12	2.14
I	(kA)	108.	108.	110.	110.
$<n_e>$	(10^{19} m^{-3})	1.2	1.2	2.1	2.1
Impurities					
Oxygen		3%	3%	3%	3%
Iron		2.‰	2.‰	0.5‰	0.5‰
Ohmic results					
$T_e(0)$	(eV)	640.	665.	600.	650.
$T_i(0)$	(eV)	~300.	180.	~480.	300.
$n_e(0)$	(10^{19} m^{-3})	2.4	2.2	4.0	3.8
τ_E	(ms)	3.1	2.7	6.0	4.8
Z_{eff}		~3.2	3.2	~2.4	2.8
V_{loop}	(V)	2.2	2.6	2.0	2.7
Results with ECH (470 kW)					
$<n_e>$	(10^{19} m^{-3})	1.2	1.2	1.7	2.1
$T_e(0)$	(eV)	2000.	2100.	1500.	1700.
$n_e(0)$	(10^{19} m^{-3})	2.0	2.2	2.6	3.6
τ_E	(ms)	2.4	2.5	3.2	4.3
Z_{eff}			3.4		3.0
V_{loop}	(V)	1.2	1.1	1.2	1.1

The effect of ECH on the density also is well illustrated by these two discharges (cf. Fig. 10). In all cases ECH leads to a strong broadening of the density profile. It is shown in Fig. 10a, corresponding to the the medium-density discharge, that this effect is only partly reproduced in the simulations. The broadening is caused both by an increase of the particle diffusion coefficient ($D_n \sim \chi_e$) and a decrease of the Ware pinch [4]. In previous simulations it was shown that these effects can explain the broadening completely, but only if a higher particle diffusivity is assumed [4]: in these simulations $D_n = 2/3\ \chi_e$. At higher densities also a net decrease of the total particle content was observed. This is illustrated by the high-density discharge (Fig.10b) in which the volume averaged density during full power ECH dropped to $\langle n_e \rangle = 1.7\ 10^{19}\ m^{-3}$. This particle pump-out is most likely due to reduced recycling during ECH. In the simulations the recycling coefficient was always kept equal to one and no attempt has been made to simulate the pump-out. The decrease of the density also largely explains the strong decrease of the energy confinement time with ECH observed in the high-density discharge.

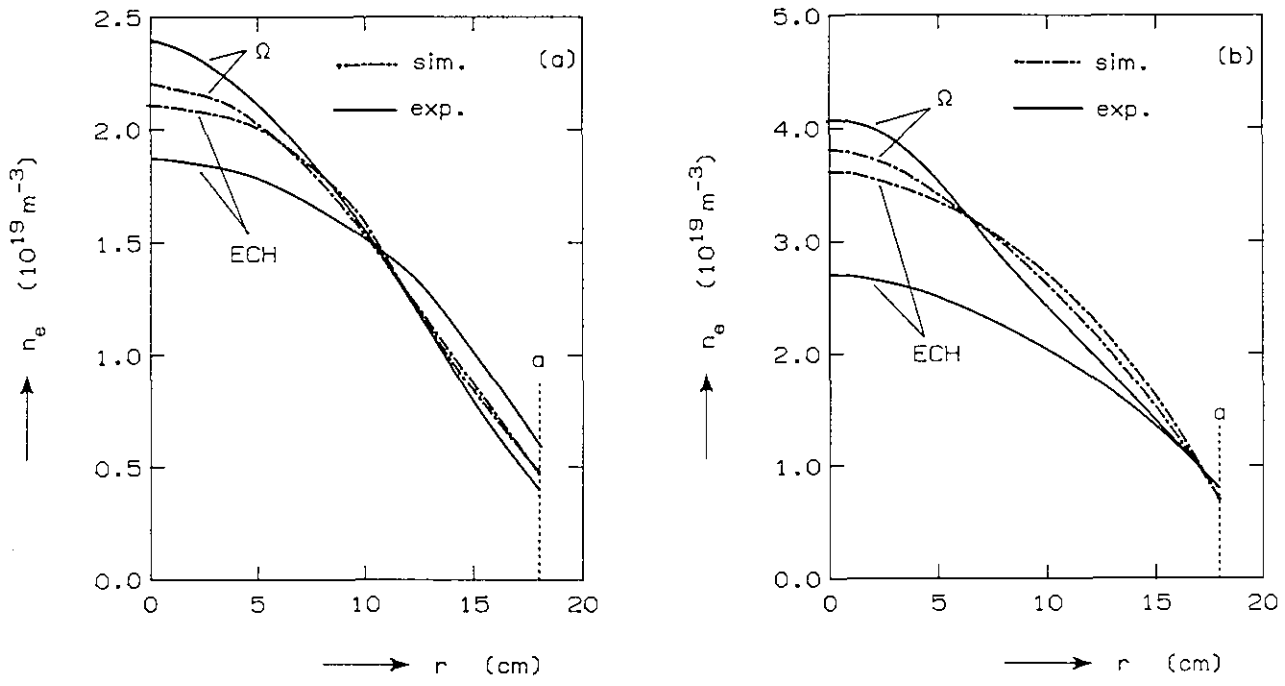

FIG. 10 The density profiles for the same discharges as in Fig. 9. Full lines represent the results of the simulations and the dashed lines the experimental data. Note the strong decrease of n_e in the ECH phase of the high-density discharge.

Off-Axis Heating.

Simulations were also performed for discharges in which the electron cyclotron resonance was placed off-axis by varying the value of the toroidal field. As an example the results of simulations of discharges with varying positions of the electron cyclotron resonance, which are otherwise equal to the medium-density discharge from the Iron-Dominated regime discussed above, are given in Fig. 11. At radii outside the electron cyclotron resonance the T_e-profiles obtained with full power ECH almost coincide with the profile obtained in the simulation for the case of central heating. At radii inside the resonance the profiles are almost flat. The reason for this result is that most EC power is deposited close to the resonance, while the power balance is completely dominated by the EC power; the energy flux outside the electron cyclotron resonance therefore is equal in all cases and, consequently, also the T_e-profiles are equal outside the resonance. This also results in a relatively moderate decrease of the energy confinement time with increasing off-axis shift of the electron cyclotron resonance. For shifts of up to ~5 cm, i.e. up to $r / a \approx 1/4$ to 1/3, this agrees with the experimental results. For larger displacements, however, a much larger decrease of the energy confinement time by a factor of ~2 was found in the experiments [5]. A possible explanation for this discrepancy is provided by tearing mode stability calculations: e.g., the broadening of the T_e-profile caused by off-axis heating with a displacement of the resonance of 8 cm led a strong destabilization of the m=2, n=1 mode, which may well cause the additional degradation of the energy confinement. These results are apparently in contrast with the ECH experiments in T-10, in which only a minor degradation of confinement was found for off-axis heating up to $r / a \approx 2/3$ [11]. A closer inspection of the data presented in Ref. [9], however, shows that the T-10 results do not refer to steady state. In fact, a large confinement degradation is found on a longer timescale, in agreement with the present results and the suggested explanation.

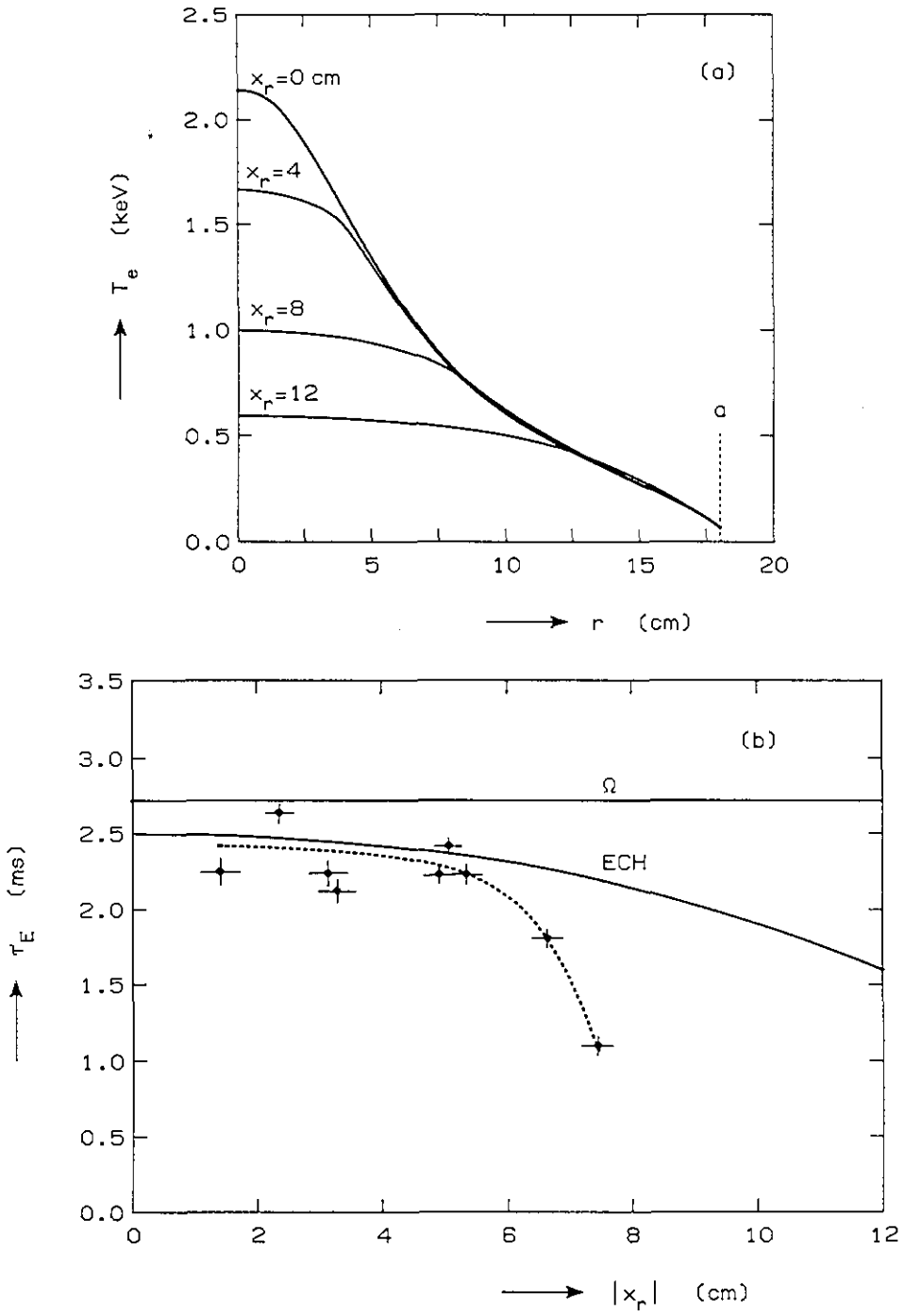

FIG. 11 Results of simulations of off-axis heating. Except for B_z all plasma parameters are equal to those for the medium-density discharge from Table 2.
a) The T_e-profiles during ECH (470 kW) for various positions of the EC resonance x_r.
b) The corresponding energy confinement time as a function of $|x_r|$. Experimental findings on the energy confinement time of medium-density discharges from the Iron-Dominated regime are indicated by the crosses and the dotted line.

3.3 CONCLUSION AND DISCUSSION.

We conclude that the $T_e^{1/2}$-scaling of the anomalous heat conductivity gives a satisfactory description of the global confinement properties of the simulated ECH experiments on TFR.

It is interesting to compare the confinement times and the anomalous heat conductivities appropriate for TFR with predictions of other scalings. As an example we compare the experimental results for the two discharges in the Low- and High-Current regimes with similar basic plasma parameters with the predictions of the scaling for Ohmic heating ('neo-ALCATOR' scaling) in the form proposed by Goldston [10]

$$\tau_E = 8.5\ 10^{-22} \langle n_e \rangle\ a^{1.04}\ R^{2.04}\ q_a^{0.5}, \tag{12}$$

which for $\langle n_e \rangle = 1.3\ 10^{19}$ m^{-3}, a = 0.18 m, R = 0.96 m, and $q_a \approx 3$ yields $\tau_E \approx 3.0$ ms. This is close to the values found in the High-Current and Iron-Dominated regimes. Goldston also has given a scaling for confinement in the presence of strong additional heating, known as L-mode scaling [10]. In the parameter range relevant for the ECH experiments in TFR, however, this L-mode scaling predicts confinement times well in excess of the predictions of Eq. (12). Under these circumstances, Eq. (12) is expected to apply also during ECH and, consequently, it is not possible to draw conclusions on the validity of L-mode scaling during ECH from the experiments on TFR alone. This could also explain the relatively small degradation, even at full (~500 kW) power ECH, in the High-Current and the Iron-Dominated regimes.

In the ECH experiments on T-10 confinement degradation was also observed to be relatively small and to be described well by the T-11 scaling for χ_e which reads [11]

$$\chi_e = 10^{20}\ \frac{T_e^{1/2}}{n_e\, q\, R\, A_i^{1/2}}\ \left[\frac{r}{R}\right]^{7/4}\ \text{m}^2/\text{s} \tag{13}$$

where A_i is the atomic weigth of the plasma ions (i.e., $A_i = 1$ for hydrogen as used in TFR). In Fig. 12 the heat conductivity of the T-11 scaling is compared to the heat conductivity in the simulations of the discharges from the Low- and High-Current regimes. We see that in the confinement range range ($r \approx 0.5$ a) the scaling for the High-Current regime (Eq. (9b)) corresponds closely to the T-11 scaling. In the Low-Current regime χ_e is smaller in this range. It must be noted, however, that the T-11 scaling for χ_e does not provide an appropriate simulation of the ECH experiments on TFR, because it predicts too small a value for χ_e at large radii (cf. Fig. 12) and, consequently, would lead to T_e-profiles which are too broad.

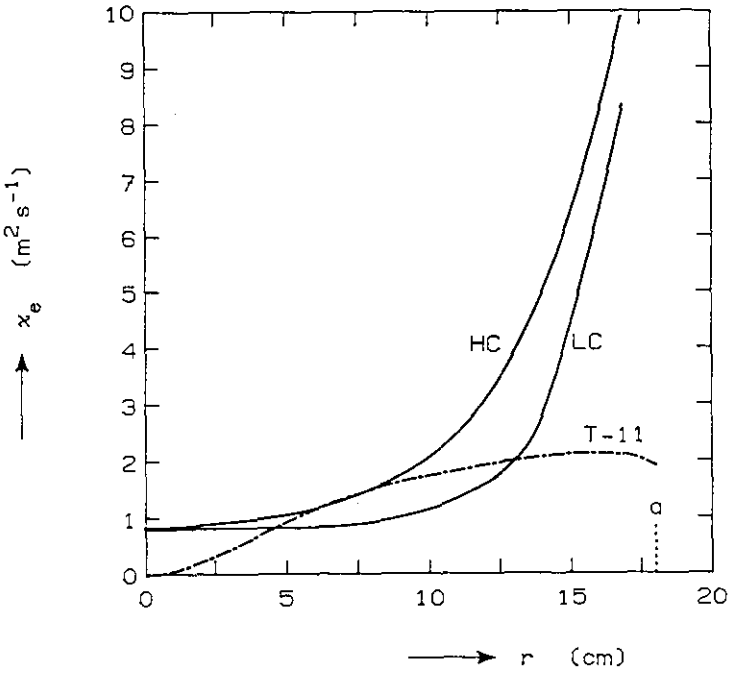

FIG. 12 The electron heat conductivity χ_e according to the Low- and High-Current scalings for the corresponding discharges from Table 1 compared with χ_e according to T-11 scaling (calculated on the basis of the profiles obtained in the simulation of the High-Current discharge).

4 MODE CONTROL.

4.1 SUMMARY OF THE EXPERIMENTAL RESULTS.

A second topic addressed in the ECH experiments on TFR was MHD mode control by local heating. Similar experiments were performed on T-10 and proved the possibility to reduce m=2 activity by local ECH [11]. The basic idea of these experiments was to reduce the temperature gradient and, consequently, the current density gradient, locally, leading to stabilization of the mode [21, 22]. The experimental results obtained on TFR were presented in Ref.s [2, 3].

The positive effect of ECH on mode activity is shown in Fig. 13: both the m=2 and m=3 activity are clearly suppressed during a full 300 ms ECH pulse (~170 kW) in a discharge which, without ECH, would exhibit strong MHD activity. The maximum efficiency was found for heating approximately 2 cm outside the q=2 surface. The exact position of the q=2 surface, however, was not known to whithin ~1cm. Experiments were also performed using a simple feedback loop which switched on ECH if the m=2 activity exceeded a preset level. An example of repeated suppression of the m=2 activity by this method is shown in Fig. 14. Also shown in this figure are the plasma displacement and the safety factor at the edge, q_a. These latter signals show that because of the increase in plasma energy with ECH and the poor position control in TFR, ECH has a strong influence on the plasma position and, consequently, on the value of q_a. This severely hampers the interpretation of the experiments.

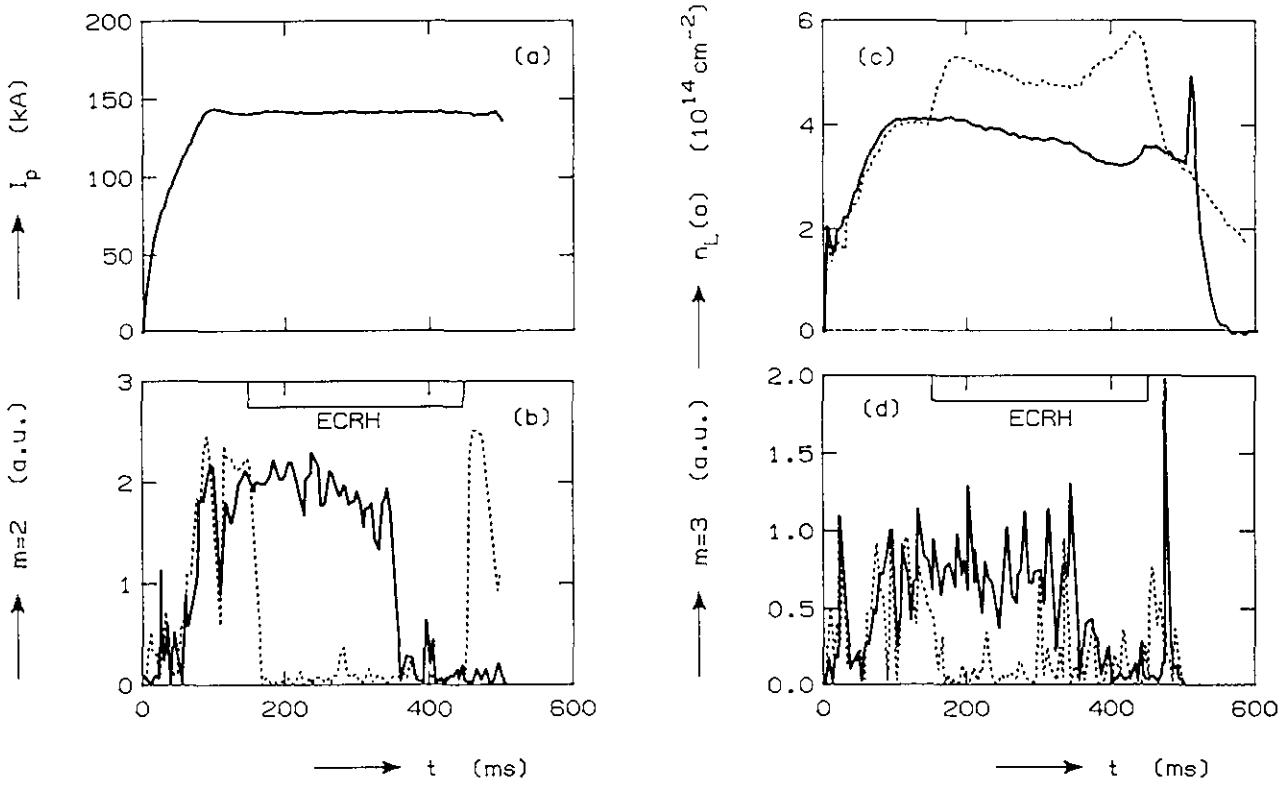

FIG. 13 An example of the suppression of MHD activity by ECH [3]. The evolution of the plasma current (a), the central line-integrated density (b), the m=2, n=1 (c) and m=3, n=1 (d) mode amplitude are given for two similar discharges, one without (full lines) and the other with a 300 ms, 170 kW ECH pulse (dashed lines). For these discharges the EC resonance was x_r=15.1 cm, the q=2 surface $r_{q=2}$=12.7 cm, and the q=3 surface $r_{q=3}$=18. cm.

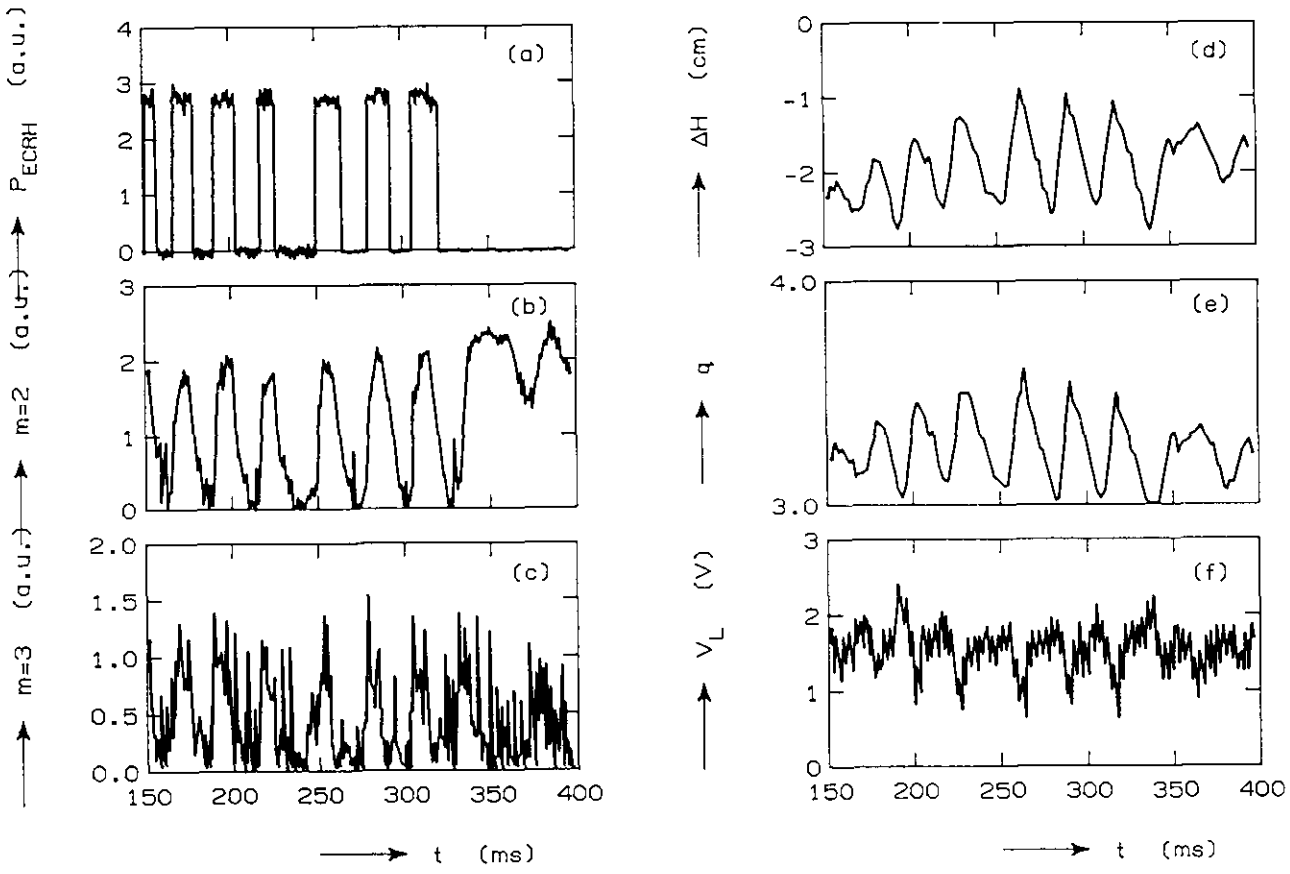

FIG. 14 An example of MHD feedback control [3]. The following signals are shown as a function of time: a) the ECH power, b) the m=2 mode amplitude, c) the m=3 mode amplitude, d) the horizontal displacement, e) the safety factor at the edge, and f) the loop voltage. For this discharge x_r=13.3 cm, $r_{q=2}$=12.7 cm, and $r_{q=3}$=18. cm.

For future applications of ECH to mode control it is important to check whether the positive results were indeed a consequence of profile tailoring. The aim of the present simulations was to answer this question. Because the m=2 activity is supposed to be due to a magnetic island around the q=2 surface which is formed by the m=2, n=1 tearing mode, we concentrated in the simulations on the effect of ECH on this mode. Moreover, the m=2, n=1 tearing mode is thought to play a dominant role in the occurrence of major disruptions (see, e.g., [23]). Especially, for a possible application of local ECH as a means of disruption control, it is thus of crucial importance to have a proper understanding of the present experimental results. In the next subsection a short description is given of the model that was employed to evaluate the evolution of the m=2, n=1 tearing mode. Then the results of the simulations are presented. In a final subsection we discuss the results and present the conclusions.

4.2 EVOLUTION OF TEARING MODES.

The evolution of the m=2, n=1 tearing mode was evaluated within the framework of quasi-linear theory (in cylindrical geometry) [12]. In order to single out the effect of profile tailoring by ECH on the mode, both the effect of island heating and the effects of the increased transport across the magnetic island were neglected. The evolution of the tearing mode with poloidal and toroidal mode numbers m and n, respectively, located at the radius r_s with $q(r_s) = m/n$, is then to a good approximation given by [12]

$$\frac{d}{dt} w_{m,n} = 1.66 \frac{\eta(r_s)}{\mu_o} \Delta'_{m,n}(w_{m,n}), \tag{14}$$

where $\eta(r_s)$ is the resistivity on r_s and $\Delta'_{m,n}(w_{m,n})$ is the jump in the logarithmic derivative of the disturbed helical flux function $\psi_{m,n}$ of the mode over the entire width $w_{m,n}$ of the magnetic island, i.e.

$$\Delta'_{m,n}(w_{m,n}) \equiv \frac{\partial/\partial r\, \psi_{m,n}(r_s+1/2\, w) - \partial/\partial r\, \psi_{m,n}(r_s- 1/2\, w)}{\psi_{m,n}(r_s)}. \tag{15}$$

The perturbed helical flux function is obtained by the integration of the following equation from 0 to r_s and from $-\infty$ to r_s with the condition of continuity of $\psi_{m,n}$ at r_s [19]:

$$\frac{d^2}{dr^2} \psi_{m,n} + \frac{d}{r\, dr} \psi_{m,n} - \left[\frac{m^2}{r^2} + \frac{\mu_o \partial j/\partial r}{B_\theta - nrB_z/mR} \right] \psi_{m,n} = 0, \tag{16}$$

where j is the current density, B_θ is the poloidal field, B_z is the toroidal field, and μ_o is the permeability of vacuum. It is seen that the mode saturates at a finite amplitude w_{sat} given by

$$\Delta'(w_{sat}) = 0. \tag{17}$$

It is noted that Δ' is a very sensitive function of the radial derivative of the current density profile. In the transport code this term depends on the assumptions made with regard to the resistivity, while the current density profile is also calculated rather crudely on the discrete radial mesh. Nevertheless, it is possible to assess certain trends in mode stability with respect to plasma parameters or the effects on mode stability due to changes in the plasma profiles caused, e.g., by local heating.

4.3 THE SIMULATIONS.

Because strong mode activity was mainly observed in discharges from the High-Current regime (see Section 3.1), we simulated discharges for which most plasma parameters were equal to those of the High-Current discharge discussed in Section 3.2. Only the toroidal field and the plasma current were increased by a factor, keeping q_a constant and shifting the electron cyclotron resonance at 60 GHz to x_r = 14 cm, i.e. we used B_z = 2.45 T and I = 130 kA. We then changed the anomalous heat conductivity in such a way that ohmic target plasmas, unstable to the m=2, n=1 tearing mode, were obtained with roughly the same energy confinement time as before. A moderately unstable target plasma ($\Delta'(0)$=4.7 m^{-1}, w_{sat} = 2.3 cm) was obtained with

$$\chi_e = 0.63\ 10^{19}\ \frac{T_e^{1/2}}{n_e}\ e^{1.6\ ((r/a)^2 - 1)}\ m^2/s. \qquad (18)$$

Whereas an only weakly unstable target plasma ($\Delta'(0)$ = 1.1 m^{-1}, w_{sat} = 1.4 cm) was obtained with

$$\chi_e = 0.7\ 10^{19}\ \frac{T_e^{1/2}}{n_e}\ e^{1.8\ ((r/a)^2 - 1)}\ m^2/s. \qquad (19)$$

In general, it is noted that increasing the factor in the exponential leads to more peaked and, consequently, more stable profiles and vice versa for decreasing this factor. TABLE 3 summarizes the results of the simulations without ECH. Note that the plasma variables for the two ohmic target plasmas show only minor differences. Yet, these differences give rise to large differences with respect to the m=2, n=1 tearing mode. The target plasmas are also not very different from the results for the High-Current discharge described in Section 3.2 (TABLE 1).

For both discharges the effect of a 100 ms ECH pulse on the unstable mode was evaluated. To study the dependence of this effect on the exact location of the heating, the wave frequency was varied between 61.0 GHz (x_r = 12 cm) and 59.4 GHz (x_r = 15 cm). The power deposition profile was calculated with a full ray-tracing calculation [18]. This was necessary, because the effect on the mode depends critically on the exact power deposition profile, while single-pass absorption was very low, typically 15 to 20% for these resonance positions, so absorption along the rays after reflection from the mirror which was mounted opposite the launchers, also had to be accounted for. During most experiments this was a tilted, mode-converting mirror (see Section 1), such that after reflection the rays had X-mode polarization. An example of the ray-tracing calculations including reflection on the tilted, mode-converting mirror is shown in Fig. 15 for the case of the moderately unstable profile and x_r = 14 cm (60 GHz). Resulting power deposition profiles are also shown in Fig. 15 for various positions of the resonance. Including the second pass the absorption was 50 to 70% (for x_r = 15 and 12 cm, resp.) indicating that most power was absorbed in the second pass. As seen in Fig. 15 this still resulted in peaked and well localized power deposition profiles as required for this type of experiments.

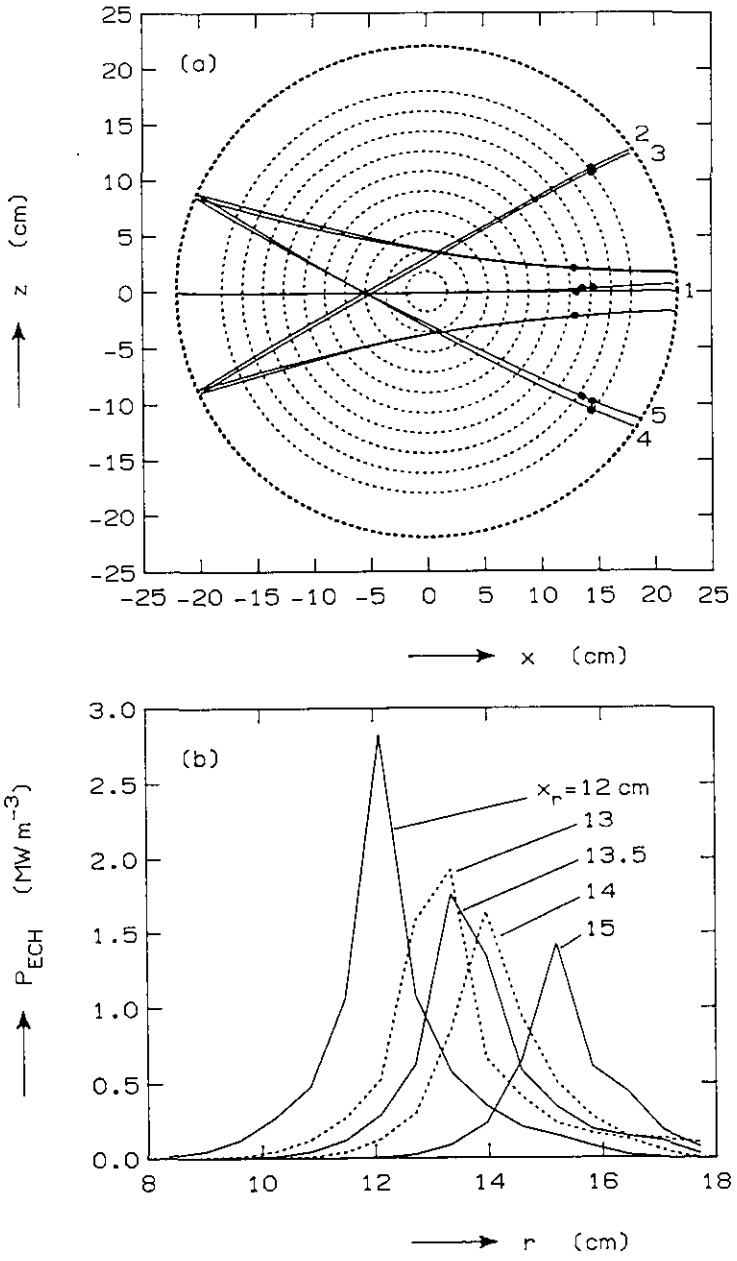

FIG. 15 Results of ray-tracing calculations for the moderately unstable case.
a) The projection of ray trajectories on the poloidal plane for the case with x_r=14. cm. The dots indicate the regions of maximum absorption along the rays. Only the central and the four outermost rays out of a set of rays that is used to model the antenna pattern, are shown. All rays were launched from R=1.5 m. The central ray was launched exactly perpendicular to the toroidal direction and the four outer rays in directions differing from the central ray by + or -3^{o} in both the toroidal and poloidal directions.
b) The calculated power deposition profiles for the five different resonance positions. Note that the power is well localized, almost exactly on r = x_r. The total absorbed power fractions are 70, 65, 60, 55, and 45% for x_r = 12.0, 13.0, 13.5, 14.0, and 15.0 cm, respectively.

TABLE 3. Results for the ohmic target plasmas.

		Moderately unstable case	Weakly unstable case
$T_e(0)$	(eV)	812.	848.
$\langle T_e \rangle$	(eV)	380.	384.
$T_i(0)$	(eV)	252.	257.
$\langle T_i \rangle$	(eV)	122.	122.
$n_e(0)$	(10^{19} m^{-3})	2.21	2.26
τ_E	(ms)	3.6	3.7
V_{loop}	(V)	2.0	2.0
q_o		0.86	0.81
$r_{q=2}$	(cm)	13.5	13.6
$\Delta'(0)$	(m^{-1})	4.7	1.1
w_{sat}	(cm)	2.3	1.4

Figure 16 shows the evolution of the width of the m=2, n=1 magnetic island, evaluated according to Eq. (14), during the injection of 300 kW of ECH (~180 kW absorbed) in the moderately unstable target plasma and for five different positions of the electron cyclotron resonance x_r. In spite of the small differences between the power deposition profiles (see Fig. 15), the effect on the evolution of the magnetic island is seen to be very sensitive to the exact position of the heating. The optimum effect, a complete suppression of the magnetic island, was obtained only for x_r = 13.5 cm, i.e. for heating almost exactly on the q=2 surface. As little as 0.5 cm difference in x_r already led to a significantly decreased effect. The stabilizing effect of ECH, however, is only temporary: 20 to 40 ms after the initial decrease of the island width, the island starts to grow again. Heating on the inside of the q=2 surface (x_r = 12 cm) even led to an increase in island width well above its initial size. A strong dependence on injected and, equivalently, absorbed power was also observed in the simulations. This is shown by the results presented in Fig. 17 for the injection of 100, 200, and 300 kW (60, 120, and 180 kW absorbed, resp.) at x_r = 13.5 cm. Also shown in this figure is the result obtained for the injection of 300 kW in the presence of the mode-conserving instead of the mode-converting mirror. The power deposition profile in this case did not differ significantly from the ones obtained in the presence of the mode-converting mirror. Only the total absorption was reduced to 30% (i.e., 90 kW), thus yielding a result intermediate between the injection of 100 and 200 kW in the presence of the mode-converting mirror.

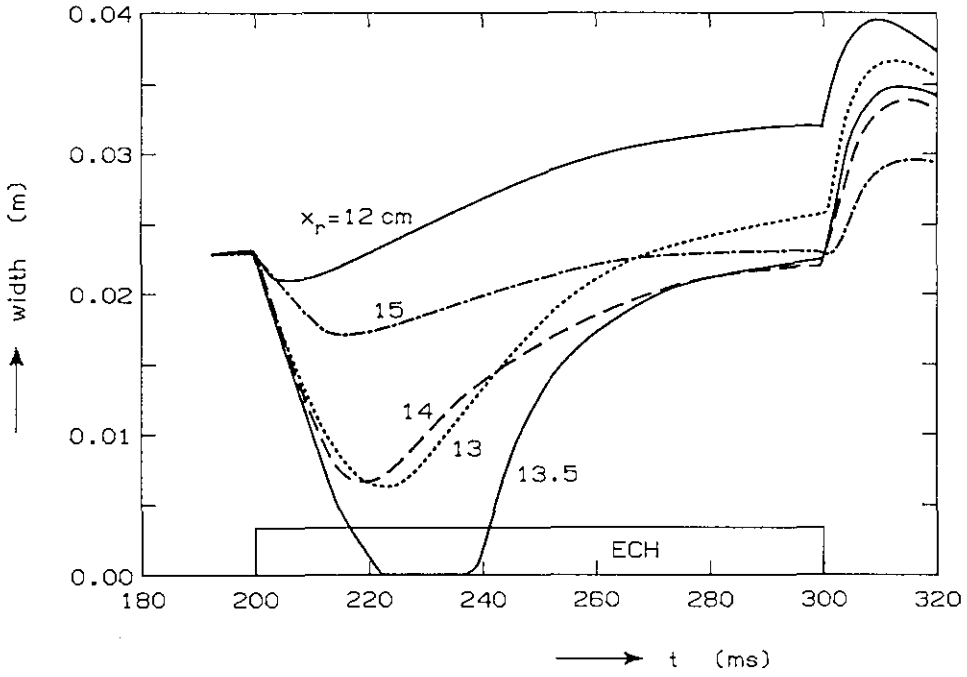

FIG. 16 The effect of ECH on the size of the m=2, n=1 magnetic island. The evolution of the island during a 100 ms, 300 kW ECH pulse is shown for the moderately unstable case and five different positions of the EC resonance.

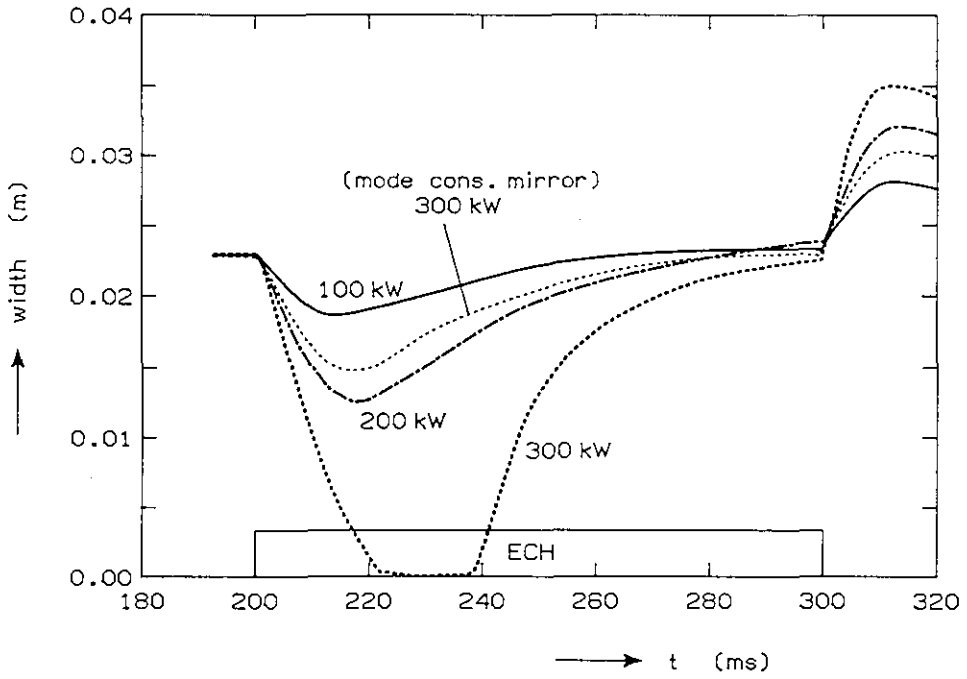

FIG. 17 As Fig. 16 but for three different levels of injected ECH power (100, 200, and 300 kW) with x_r = 13.5 cm. Also the effect of the injection of 300 kW in the presence of the mode-conserving instead of the mode-converting mirror is shown. In this case the absorbed power was only 90 kW, while the deposition profile was not significantly different from the cases with the mode-converting mirror.

In the case of the weakly unstable target plasma the results were slightly less sensitive to x_r. As shown in Fig. 18 for injection of 300 kW (~180 kW absorbed), complete suppression of the magnetic island was obtained for x_r =13, 13.5, and 14.5 cm. Again this suppression was only temporary, although for x_r = 13 or 13.5 cm the island starts to grow again after a much longer time of ~80 ms. The dependence on injected power was similar to the case of the moderately unstable target plasma: injection of either 100 or 200 kW at the optimum value of x_r = 13.5 cm did not lead to complete suppression of the magnetic island.

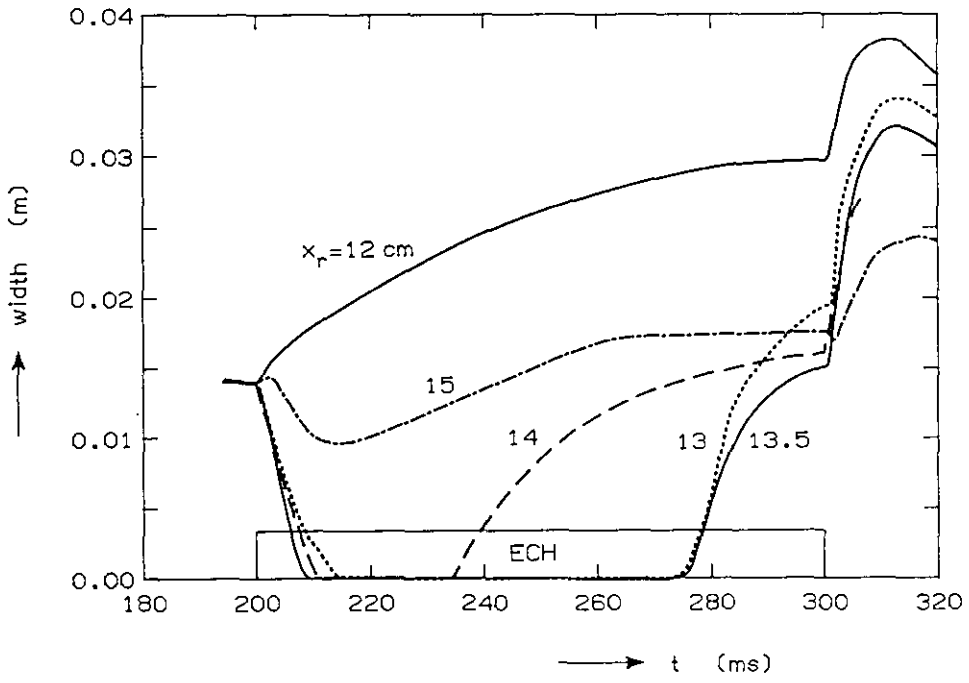

FIG. 18 As Fig. 16 but for the weakly unstable case. Note that in this case the mode is more easily stabilized. The stabilization is again only temporary.

4.4 DISCUSSION AND CONCLUSION.

Comparing the results of the simulations with the experimental data the following differences are immediately apparent. First, the optimum results in the experiment were obtained by heating approximately 2 cm outside the q=2 surface [3], while the best results in the simulations were obtained for heating almost exactly on the q=2 surface. It is even noted that the experimental parameters corresponding to Fig. 13 ($r_{q=2} \approx 13$ cm and $x_r = 15$ cm) closely resemble those for the simulations with $x_r = 15$ cm which showed hardly any suppression of the island. Secondly, in the simulations the injection of 300 kW was required for complete stabilization while in the experiments suppression of the MHD activity was easily obtained with one gyrotron, i.e. ~170 kW. A possible reason for this discrepancy is that only around 60% of the power is accounted for in the simulations while in the experiment the remaining 40% may well have been absorbed after multiple reflections or conversion to Bernstein waves at the upper-hybrid resonance. If these 40% are absorbed close to the resonance with a deposition profile similar to that of the power absorbed in the first and second pass, one should rather compare results of simulations and experimental results taking the absorbed power equal to the injected power. In that case, one finds that one gyrotron (~170 kW) could be sufficient to obtain complete suppression of the magnetic islands in the experiments. Finally, in the simulations the island suppression was only temporary while in the experiment the MHD activity could be suppressed for a full 300 ms pulse of ECH (cf. Fig. 14). This discrepancy is more serious since there is a very simple reason for it, which is directly related to the nature of the profile changes that can be obtained by local heating. This is illustrated by Fig. 19 which gives the temperature and the current density profile before ECH, 10 ms after the start of ECH and at the end of the 100 ms ECH pulse for the injection of 300 kW at $x_r = 13.5$ cm in the case of the moderately unstable profile. After 10 ms of ECH the changes of the current density profile are mainly localized around x_r and such that $\Delta'(0)$ is well below zero (stable case) due to the clearly visible reduction of the current density gradient around $r_{q=2}$. At that time the island size is still finite, because it changes only on a local resistive timescale (cf. Eq. (14)) and, consequently, lags behind. On a longer timescale the changes of the current density profile are more global and a strong broadening of j(r) takes place, induced by the broadening of the temperature profile. This broadening of the current density profile is, in general, destabilizing to the m=2, n=1 tearing mode.

We are led to the conclusion that the suppression of the MHD activity with ECH obtained in the experiments on TFR cannot be due to current profile tailoring alone. This conclusion is also supported by experimental data as presented in Fig. 15 which show a clear correlation between plasma position (i.e. q_a) and the MHD activity. This may well have the same origin as the correlation between q_a and MHD activity that descriminates the High-Current and the Low-Current regimes (cf. Section 3).

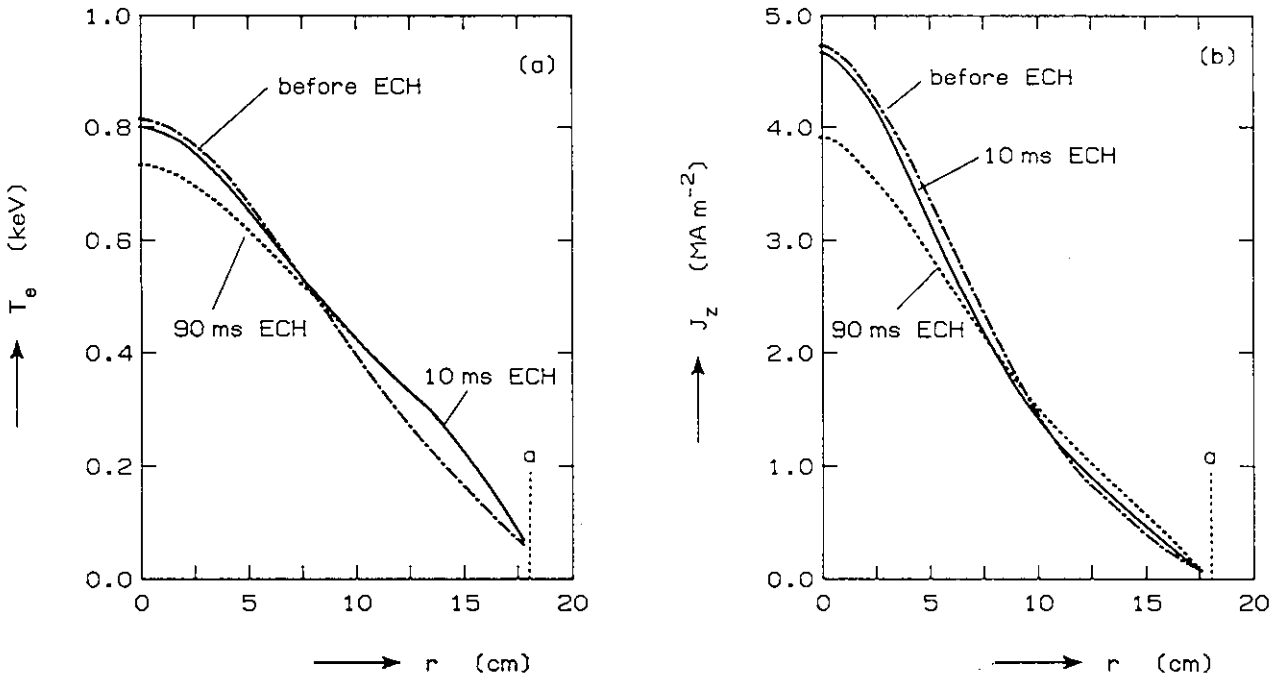

FIG. 19 The effect of ECH on the temperature (a) and the current density (b) profiles. The profiles before ECH, after 10 ms ECH, and at the end of the ECH phase are given for the moderately unstable case with 300 kW of ECH at x_r = 13.5 cm. Note that after 10 ms the changes in the current density profile are still well localized around r = x_r leading to the stabilization of the mode. On a longer time scale, however, the current density profile is significantly broadened which causes the mode to become unstable again.

5 SUMMARY AND CONCLUDING REMARKS.

Transport code simulations of the ECH experiments performed on TFR were carried out. Both bulk heating and MHD mode control were addressed. Three experimental plasma regimes were identified, namely, the Low- and High-Current and Iron-Dominated regimes [4-6], an anomalous electron heat conductivity, χ_e, scaling like $\chi_e \sim T_e^{1/2} / n_e$ yielded a good simulation of the respective ohmic phases. In the High-Current and Iron-Dominated regimes the observed degradation of confinement with ECH was adequately described by the $T_e^{1/2}$ scaling of χ_e. In the Low-Current regime wich during the ohmic phases was characterized by an exceptionally high confinement [2, 3, 6], a much larger degradation of confinement was found, even at low-power ECH. In fact, during ECH discharges in the Low- and High-Current regimes were almost indistinguishable, and the scaling of the High-Current regime also gave a good description of the ECH phases of Low-Current discharges. Around $r \approx 0.5$ a, i.e. in the so-called confinement range, the High-Current scaling is similar to T-11 scaling [11], both in absolute value and with respect to the scaling with T_e and n_e. These results confirm those obtained in T-10 in which the degradation of confinement with ECH was shown to be less then predicted by L-mode scaling [10] but to agree with T-11 scaling [9, 11]. The L-mode scaling, however, does not apply in the parameter range covered by the experiments in TFR. Consequently, a definite conclusion regarding the question whether the behaviour of the energy confinement with ECH is similar to or more favourable than that for other heating methods, cannot be drawn from the TFR results.

The behaviour of the m=2, n=1 tearing mode was studied both in view of the differences between the High- and Low-Current regime and of the MHD mode control experiments. Contrary to the experimental observations, the profiles obtained with High-Current scaling were found to be more stable than those obtained with the Low-Current scaling for χ_e. The MHD mode control experiments were simulated within the framework of the quasi-linear theory for tearing modes [12]. Both the dependence on the position of the electron cyclotron resonance and the injected power were studied. The results were found to depend very sensitively on the position of the resonance. A complete suppression of the m=2, n=1 magnetic island was obtained for heating almost exactly on the q=2 surface, while varying the resonance position by as little as 0.5 cm had a much weaker effect. The suppression of the magnetic island was in all cases found to be only temporary. These results are in contrast with the experiments [3] in which the optimum effect was obtained for heating approximately 2 cm outside the q=2 surface, and the suppression of the MHD activity lasted for a full 300 ms pulse of ECH. The interpretation of these experiments is, however, difficult because of the strong effect ECH has on the horizontal plasma position. In fact, in many cases a clear correlation between q_a and the MHD activity was observed, similar to the one discriminating the High- and Low-Current regimes [2, 3]. These results show that stability or instability of the m=2, n=1 mode is a consequence of more complicated (non-linear) effects, rather than being determined by linear tearing mode theory. One possibility is that the m=2, n=1 mode is driven unstable by the m=3, n=1 ideal kink mode which is expected to be unstable for q_a close to 3 [20].

ACKNOWLEDGEMENTS.
The members of the TFR-Group and colleagues from the FOM-ECRH-Team are gratefully acknowledged for many discussions on the experimental data and their interpretation. In particular we would like to thank Drs. M.A. Dubois and J.A. Hoekzema for their continuing interest in this work. Also discussions with Prof. F. Engelmann are gratefully acknowledged. This work was performed under the Euratom-FOM association agreement with financial support from ZWO and Euratom.

REFERENCES.

[1] CANO, R., CAPES, H., DUBOIS, M., ORNSTEIN, L.Th.M., SCHRADER, W.J., et al., in proceedings of 4th Int. Symp. on Heating in Toroidal Plasmas, Rome (Italy), 21-28 March (1984), Vol. II p. 853.
[2] FOM-ECRH-TEAM, TFR-GROUP, paper contributed to 12th Eur. Conf. on Contr. Fusion and Plasma Physics, Budapest (Hungary), 2-6 Sept. (1985), Vol II p. 60.
[3] TFR-GROUP, HOEKZEMA, J.A., et al., in proceedings of 5th Int. Workshop on Electron Cyclotron Emission and Electron Cyclotron Heating, San Diego (USA), 9-12 Nov (1985), p. 154.
[4] TFR-GROUP, FOM-ECRH-TEAM, paper contributed to 13th Eur. Conf. on Contr. Fusion and Plasma Heating, Schliersee (FRG), 14-18 April (1986), Vol. II p. 207.
[5] DE ESCH, H.P.L., et al., EQUIPE-TFR, in Plasma Physics and Controlled Nuclear Fusion Research (Proc. 11th Int. Conf. Kyoto, 1986), Vol. 1, IAEA, Vienna (1987) 559.
[6] HOEKZEMA, J.A., FOM-ECRH-GROUP, TFR-GROUP, invited paper KIEV 1987
[7] RIVIERE, A.C., Plasma Phys. Contr. Fusion **28** (1986) 1263.
[8] BURRELL, K.H., PRATER, R., EJIMA, S., ANGEL, T., ARMENTROUT, C.J., et al., in Plasma Physics and Controlled Nuclear Fusion Research (Proc. 10th Int. Conf. London, 1984), Vol. 1, IAEA, Vienna (1985) 131.
[9] KADOMTSEV, B.B., Plasma Phys. Contr. Fusion **28** (1986) 125.
[10] GOLDSTON, R.J., Plasma Phys. Contr. Fusion **26** (1984) 87.
[11] ALIKAEV, V.V., ARSENTIEV, Yu.I., BAGDASAROV, A.A., BEREZOVSKIJ, E.L., BORSHEGOVSKIJ, A.A., in Plasma Physics and Controlled Nuclear Fusion Research (Proc. 10th Int. Conf. London, 1984), Vol. 1, IAEA, Vienna (1985) 419.
[12] WHITE, R.B., MONTICELLO, D.A., ROSENBLUTH, M.N., WADDELL, B.V., Phys. Fluids **20** (1977) 800.
[13] WATKINS, M.L., HUGHES, M.H., ROBERTS, K.V., KEEPING, P.M., KILLEEN, J., Methods Comput. Phys. **16** (1976) 165.
[14] HINTON, F.L., HAZELTINE, R.D., Rev. Modern Physics **48** (1976) 239.
[15] HUGILL, J., Nucl. Fusion **23** (1983) 331.
[16] BORNATICI, M., CANO, R., DE BARBIERI, O., ENGELMANN, F., Nucl. Fusion **23** (1983) 1153.
[17] CANO, R., CAPES, H., HA QUANG, D., MERCIER, C., MORERA, J.P., 'Code de calcul du dépot de puissance d'une onde résonnante a la fréquence cyclotronique électronique', Report EUR-CEA-FC-1170 (1983).
[18] KRITZ, A.H., HSUAN, H., GOLDFINGER, R.C., BATCHELOR, D.B., in proceedings of 3rd Int. Symp. on Heating in Toroidal Plasmas, Grenoble (France), 22-26 March (1982) Vol. II p. 707.
[19] FURTH, H.P., RUTHERFORD, P.H., SELBERG, H., Phys. Fluids **16** (1973) 1054.
[20] WESSON, J.A., Nucl. Fusion **18** (1978) 87.
[21] HOLMES, J.A., CARRERAS, B., HICKS, H.R., LYNCH, S.J., WADDELL, B.V., Nucl. Fusion **19** (1979) 1333.
[22] CHAN, V., GUEST, G., Nucl. Fusion **22** (1982) 272.
[23] WADDELL, B.V., CARRERAS, B., HICKS, H.R., HOLMES, J.A., LEE, D.K., Phys. Rev. Lett. **41** (1978) 1386.